ANKARA YILDIRIM BEYAZIT UNIVERSITY

GRADUATE SCHOOL OF NATURAL AND APPLIED SCIENCES

A DEVICE TO MEASURE THAT THE PUNCTURE CURRENT OF INSULATION THAT CABLE EXPOSED TO HIGH VOLTAGE AND HIGH FREQUENCY

M.Sc. Thesis by

Merve Gülşah KARAKAŞ

Department of Defense Technologies

February, 2021

ANKARA

A DEVICE TO MEASURE THAT THE PUNCTURE CURRENT OF INSULATION THAT CABLE EXPOSED TO HIGH VOLTAGE AND HIGH FREQUENCY

A Thesis Submitted to

The Graduate School of Natural and Applied Sciences of

Ankara Yıldırım Beyazıt University

In Partial Fulfilment of the Requirement for the Degree of Master of Science in Defence Technologies Department

By

Merve Gülşah KARAKAŞ

February, 2021

ANKARA

M.Sc. THESIS EXAMINATION RESULT FORM

We have read the thesis entitled **‘‘A DEVICE TO MEASURE THAT THE PUNCTURE CURRENT OF INSULATION THAT CABLE EXPOSED TO HIGH VOLTAGE AND HIGH FREQUENCY’’** completed by **MERVE GÜLŞAH KARAKAŞ** under supervision of **Assoc. Prof. Dr. SİNAN KIVRAK** and we certify that in our opinion it is fully adequate, in scope and in quality, as a thesis for the degree of Master of Science.

Assoc. Prof. Dr. Sinan KIVRAK

Supervisor

Prof. Dr. Kamil Çağatay BAYINDIR

Jury Member

Assoc. Prof. Dr. Selim ÖNCÜ

Jury Member

Prof. Dr. Ergün ERASLAN

Director

Graduate School of Natural and Applied Sciences

ETHICAL DECLARATION

I hereby declare that, in this thesis which has been prepared in accordance with the Thesis Writing Manual of Graduate School of Natural and Applied Sciences,

- All data, information and documents are obtained in the framework of academic and ethical rules,
- All information, documents and assessments are presented in accordance with scientific ethics and morals,
- All the materials that have been utilized are fully cited and referenced,
- No change has been made on the utilized materials,
- All the works presented are original,

and in any contrary case of above statements, I accept to renounce all my legal rights.

Date: …………….. **Signature:………………………………………..**

Name & Surname: Merve Gülşah KARAKAŞ

ACKNOWLEDGEMENTS

I would like to express my gratitude to my supervisor, Assoc. Prof. Dr. Sinan KIVRAK for his continuous support and motivation during my study. His knowledge, invaluable experiences and priceless advices constructed the milestones of my thesis study. It was a pleasure to work with him.

I express my sincere love and special thanks to my mother, father, sister and my the biggest supporter my husband Hasan KARAKAŞ for their sincere prayers, supports, courage and patience for me.

2021, February Merve Gülşah KARAKAŞ

A DEVICE TO MEASURE THAT THE PUNCTURE CURRENT OF INSULATION THAT CABLE EXPOSED TO HIGH VOLTAGE AND HIGH FREQUENCY

ABSTRACT

One of the most important issues in high voltage conductors is the puncture voltage point of the insulation used in the conductor. In the design of a system with high voltage, the puncture voltage of this insulation is of great importance. In this thesis, the design and application of a system that determines the puncture voltage-frequency point of enamel coated coil wires is explained. The system determines the puncture stress point of the plating by applying an AC square signal of 1 - 5000 V / 1 - 5000 Hz to a twisted and open-clad enameled conductor until puncture occurs within the desired range. The mains voltage is adjusted via a Variac so that the applied electrical signal reaches the desired peak voltage. Then, the signal received from the output of variac is passed through a rectifier circuit and connected to the DC bus voltage of the H-Bridge circuit. The AC square signal obtained from the H-Bridge circuit is folded in a high frequency transformer so that the desired signal is obtained in the secondary winding of the transformer. The high voltage signal applied to the conductor increases the current passing through the primer of the transformer when the insulation is short circuit. The signal in the transformer can be controlled with the help of a processor, as it is understood that the puncture occurs with the current value read from the primary. Finally, the system design was simulated in the PSIM program and compared with the experimental results. The experiment results and simulation results are in harmony.

Keywords: High voltage, puncture voltage, enamel, coil wire

YÜKSEK VOLTAJ VE YÜKSEK FREKANSA MARUZ BIRAKILAN KABLOLARIN İZOLASYON DELİNİMİNİ ÖLÇEN BİR CİHAZIN TASARIMI VE UYGULAMASI

ÖZ

Yüksek gerilim iletkenlerindeki en önemli hususlardan biride iletkende kullanılan izolasyonun, delinme gerilimi noktasıdır. Yüksek gerilimin bulunduğu bir sistemin tasarımında bu izolasyonun delinme gerilimi büyük önem arz etmektedir.

Bu tezde temel alınan emaye kaplı bobin tellerinin delinme gerilim-frekans noktasını tespit eden bir sistemin tasarımı ve uygulaması yapılmıştır. Sistem, burgulanmış (twistlenmiş) ve uçları açık devre edilmiş emaye kaplı bir iletkene, 1 – 5000V / 1 – 5000Hz‘lik AC kare sinyali, istenilen aralıkta delinme gerçekleşene kadar uygulayarak kaplamanın delinme gerilim noktasını tespit etmektedir. Uygulanan elektriksel sinyalin, istenilen tepe gerilimini elde etmesi için şebeke gerilimi bir Varyak aracılığıyla ayarlanabilir hale getirilir. Daha sonra Varyak’ın çıkışından alınan sinyal, bir doğrultucu devreden geçirilerek H-köprü devresinin DC bara gerilimine bağlanır. H-Bridge devresinden elde edilen AC kare sinyal, bir yüksek frekans transformatöründe katlanır ve böylece transformatörün sekonder sargısında istenilen sinyal elde edilmiş olunur. İletkene uygulanan yüksek gerilim sinyali, izolasyon kısa devre olduğunda transformatörün primerinden geçen akımı arttırmaktadır. Primerden okunan akım değeri ile delinmenin gerçekleştiği anlaşılarak transformatördeki sinyal, işlemci yardımıyla kontrol edilebilmektedir.

Son olarak sistem tasarımı PSIM programında simüle edilerek deney sonuçları ile karşılaştırılmıştır. Deney sonuçları ile simülasyon sonuçları bir uyum içerisindedir.

Anahtar Kelimeler: Yüksek gerilim, delinme gerilimi, emaye, bobin teli

CONTENTS

NOMENCLATURE

Acronyms

PSIM	Powersim Electronic Simulation Software
AC	Alternating Current
DC	Direct Current
HV	High Voltage
PVC	Polivinil Chloride
VPE-XLPE	Cross-linked polyethylene
PWM	Pulse Width Modulation
RMS	Root Mean Square
ADC	Analog to Digital Converter
HFT	High Frequency Transformer
MCU	Microprocessor Control Unit
R_{ds}	MOSFET Drain-Source Resistance
F	Farad

LIST OF TABLES

LIST OF FIGURES

CHAPTER 1

INTRODUCTION

1.1 Literature Review

M. Kaufhold et al., in an article published in 1996, examined the insulation damages caused by partial discharge in low and medium voltage induction motors and how the insulation design is affected by temperature and applied voltage [1].

In an article published by Weijun Yin in 1997, partial discharges caused by voltage rises borned of impedance mismatch between the inverter and the motor used in low voltage induction motors were examined [2].

D. Fabiani et al. conducted a study similar to this thesis in an article published in 2001. They performed a partial discharge test by applying a square wave voltage ranging from 50 HZ to 10 kHz to conductor pairs covered with three different insulation materials [3].

In an article published by A. Cavallini et al. in 2001, they examined the damages caused by partial discharge on enamel coated wires used in electric motors [4].

Considering the studies conducted on high voltage puncture and test systems, a study by Fabiani, Davide et al. in 2004, found a useful feedback to enameled conductor manufacturers on the selection of additional structure and enamel components through direct field load measurement by showing experimental evidence on the relationship of partial discharge with load accumulation on enamelled conductors, and as a result of their study [5].

A study by Ozaki, Tamon et al. carried out in 2005, on the damage of enamel conductors used in motors due to partial discharge. An enamel coated conductor hybridized with nanoscale inorganic particles was prepared in this study [6].

A study by Saeed UI Haq in 2007 examined the damage caused by high stresses caused by inverter type asynchronous motor drives to the windings of the motor [7].

A. Cavallini et al. conducted a study in 2011 on the causes of partial discharge in systems using enamelled conductors such as induction motors and transformers [8].

In his study in his master's thesis in 2013, Fatih ISSI ensured that the grounding resistance was kept constant in the grounding systems with the dsPIC controlled H-Bridge structure [9].

Daniel J.T. studied the effects of mechanical stresses that enamel insulated copper conductors will be exposed to during motor winding manufacturing, on the electrical performance of the insulation. In this context, they conducted experiments on the initial voltage of partial discharge, and within the scope of these experiments they carried out in 2013, they examined rectangular cross-section, non-stress and tensile, enamel-insulated copper conductors and compared their breakdown voltages and partial discharge behaviors [10].

Wang Peng, Andrea Cavallini, and Gian Carlo Montanari conducted on a study on the effect of recurrent square wave voltage on enamel-coated conductor durability in 2014. It was found that enamelled conductors can be significantly affected by the parameters of the signal (rise time and frequency) applied to the conductor [11].

Hasan Ali YILDIZ conducted a study on examining the drilling processes of solid and liquid insulation materials used in power transformers in his doctorate thesis in 2014 [12].

In their study in 2017, Shinya Ota et al examined the damage caused by partial discharge to isolated systems due to the application of a high frequency voltage. They then worked on a new magnet wire coated with a porous insulator to increase the surge resistance as a solution to this damage [13].

In their study in 2018, Ewa N., Sonia A., and Daniel R. created ac motor windings without partial discharge by adding a thin conductive layer to the outer surface of the enameled wire used to form the machine winding. During this study, they examined the Paschen hypotheses, as a result, they showed that it was possible to strongly reduce partial discharge by adding small amounts of varnish to critical areas [14].

Sonia A, Daniel R. and Emmanuel M. analyzed the improvement stages of a PWM powered motor insulation in 2019 to examine the effect of semiconductor quality on partial discharge. In their study, they made simulations to understand the behavior of three different types of enameled wires against high voltage [15].

Moein B. and Mona G. studied the vulnerability of silicon gel to high-speed square voltage pulses in their model developed in 2019. Using the model, they studied the effect of frequency and spin ratio on the magnitude and velocity of PD events [16].

P. Seri et al., in the study they conducted in 2020, examined the theoretical and experimental differences of the partial discharge measurement method, and analyzed the internal defect conditions they obtained as a result. As input to this analysis, they created a simple mathematical model for a true defective insulation and experimental validation on XLPE and polypropylene [17].

In his study in 2020, Marek Florkowski used various sample combinations to reveal the material resistance effect on partial discharge activity. In this way, he investigated the role of dielectric properties of insulation materials in partial discharge, and investigated the effect of static in the initial stage and charging stage [18].

1.2 Objectives of the Thesis

This thesis study aims to find the puncture stress points of the insulation materials used in conductors under variable frequency. In the system to be designed, the DC bus voltage of the H-Bridge structure is taken from a single phase variac. The output of variac is connected to the DC bus voltage of the H-Bridge switching circuit by passing a rectifier circuit. In this way, 220 V (AC) mains voltage can be adjusted in the range of 1-310 V (DC). With the H-Bridge switching circuit, the frequency value of the output voltage can be adjusted between 1 and 5000 Hz. The output voltage can be increased up to 5000 V with a high frequency transformer with a conversion ratio of 1:20, which is also connected to the H-Bridge circuit as a load. The system performs H-Bridge switching, reading of the input current of the high frequency transformer and measuring the puncture voltage with a microprocessor control card.

CHAPTER 2

INSULATOR TYPE

2.1 Wire Insulator

Studies on the effects of electricity on the human body have shown that 50 mA of electric current can cause heart attacks, skin diseases and high mortality. The types of insulators used in cabling and cables are of great importance in both human health and applications especially in terms of high voltage. In order to be able to say well to the insulation resistance of cable cores, it is necessary to measure and evaluate high resistance requirements. The answer to the question of whether it is good in evaluation is hidden in measuring the insulation resistance [19].

No insulating material provides endless resistance. Since insulations can be used from practical purposes to the most critical situations, their tolerances should be determined and evaluated accordingly. The insulation resistances of the cable cores are given in the relevant production standards [19].

The measurement of insulation resistance is based on Ohm's Law. In calculating the resistance value, a constant voltage is applied to the system and the current value is measured during this time. The voltage and current ratios applied enable us to obtain insulation resistance [19].

2.2 Insulating Materials and Dielectric Properties

A material to be used as an insulator should have high resistivity and puncture resistance and a small dielectric constant. The resistivity of an insulating material is over 10^{10} ohms / m, and its puncture strength is between 10-20 kV / mm. The most suitable material produced with today's technology for the insulation of conductors is polymer. Despite being easy and cheap to manufacture, they are not suitable for high temperature applications. Thermoplastics, in particular, soften easily with temperature [20].

2.2.1 Dielectric Constant

Electrical polarization causes the accumulation of charge on the surface of the material. If there is permanent polarization in the dielectric material, the load accumulation occurs automatically. When an electric field is applied to an element that does not have permanent polarization, polarization occurs with external influence. Therefore, electrical charge accumulation occurs on the surface. In both cases, the charge density on the surface is proportional to the electric field intensity [20].

The electrical charge density q is defined as the number of electrons accumulated in $1cm^2$. The distance (electrode opening) a (cm) between two conductive boards parallel to each other and the applied voltage U (volt) is the electric field intensity (**E**) between them;

$$\boldsymbol{E} = U / a \ (F/m) \quad \textbf{(2.1)}$$

If there is a gap between the boards, electrical charge density;

$$q_0 = \varepsilon_0 \ x \ \boldsymbol{E} \quad \textbf{(2.2)}$$

If there is any insulating material between the conductive boards, electrical charge density;

$$q_m = \varepsilon_m \ x \ \boldsymbol{E} \quad \textbf{(2.3)}$$

Here ε_m is the dielectric constant of the material. As ε_m grows, the capacity of the cable C_k also increases. As C_k increases, it's capacitive reactance $X_k = 1 / \omega C_k$ decreases. As X_k decreases, the current passing through the conductor increases and the lost energy increases. The physical properties of some materials are given in Table 2.1 [20].

Table 2.1 The physical properties of some materials [20]

MATERIAL	Ɛ (Farad/meter)
PVC	4.0
Silicone	3.2
Rubber	4.82
VPE-XLPE	2.26
Enamel	9.0

2.2.2 Insulating Materials Frequently Used in Cables

2.2.2.1 PVC

PVC is the most common type of insulation with very cheap and wide usage area. It is highly resistant to chemicals, corrosion, impacts, abrasion and weather conditions. The temperature ranges from -40 ° C to 150 ° C [21].

2.2.2.2 Silicone

Silicone has a very flexible and heat resistant structure. It is suitable for use in environments between 75°C and 250°C. The disadvantages are that they are expensive and static [21].

2.2.2.3 Rubber

Rubber is a material with similarity like silicone and PVC. It has better abrasion resistance than silicone, but not as chemically resistant as PVC. It is more suitable for outdoor and industrial environments. The temperature of use ranges between -25°C and 60°C [21].

2.2.2.4 VPE-XLPE

Cross-linked polyethylene (VPE-XLPE) is used as insulating material in power cables. High improvements have been achieved in areas such as tensile strength and shape retention at high temperatures, as well as increased strength, impact resistance and resistance to solvents by using cross-linked materials in the cable production technique [21].

2.2.2.5 Enamel

Enamel is a solid substance with a brilliant appearance obtained through applying the solution made up of a mixture of some inorganic oxides onto the metallic or cast surface and then firing these oxides at the melting temperature. Despite being defined as "enamel", neither an enamel paint layer nor a vitreous glass powder made of molten glass is coated with enamel. Enamelled wire insulation usually consists of two layers includinga base coat and a top coat. The materials used to create these layers are often Polyester-Imit (PEI) and Polyamide-Imit (PAI), both of which are high temperature resistant materials with stable thermal properties. The glass transition temperature (Tg) for both materials is about 270 ° C [21].

2.2.2.5.1 *What is Enamel Coated Wire?*

Enamelled wire is electrical equipment resistant to moisture, aggressive chemicals and high temperature, in addition to its ability to transmit high voltage by coating varnish (enamel) on the conductive wire surface. Electrolytic copper is generally used as a conductive wire. Blister copper with high copper content but impurities (non-homogeneous) is firstly refined at 1250 ° C in the anode casting plant. As a result of this process, copper, whose purity is close to 99%, cannot be used in places requiring high conductivity due to impurities in it. Electrolysis is applied for further copper purification. Copper cathode with 99.99% purity is obtained from the copper anode by electrochemical method. The obtained high purity copper cathode is melted in continuous casting plants and 8mm wire rod is obtained by casting. Wire rods of 8 mm are pulled to wires with lower diameters in wire drawing units and wrapped in large baskets to be connected to enamelling machines [21].

Electrolytic copper wire with 99.99% purity attached to the enamelling machine enters the wire drawing unit again to achieve the desired final diameter. The copper wire, which is extended by 26% in each pass, passes through the exit roll and becomes quite hard due to the mechanical effect it is exposed to. The wire enters the annealing unit in the range of 500 - 700 ° C to regain softness and flexibility. Liquid varnish is applied to the wire coming out of annealing with the help of enamel rollers. During the passage through the oven, the solvent in the varnish flies, leaving solid varnish on the wire. Wire is passed through the oven by applying varnish several times until the appropriate enamel thickness is gained and at the end of the process, it is wound on the reel [21].

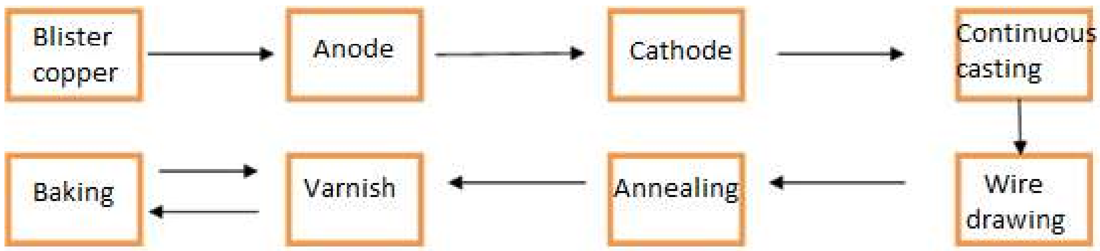

Figure 2.1 Enamel coated wire production process [21]

2.2.2.5.2 What Are the Uses of Enamel Coated Wire?

The usage areas of enameled wires vary according to the conductor diameter and the type and temperature classes of the coating on it. IEC, NEMA, DIN standards are referenced in enameled wire productions [21].

Generally, their usage areas are given in Table 2.2.

Table 2.2 Enamel coated wire's usage areas [21]

Temperature class	**Some Uses**
155 °C	Contactor, small motors and transformers, relays and solenoids
180 °C	Electric motors, ignition coils, wiper motors, transformers
200 °C	Generators, winding coils, general purpose motors, brake systems
220 °C	Refrigerator motor, distribution transformers, oil immersed transformers, compressors

2.3 How to Calculate the Insulation Resistance?

A constant voltage is applied to the system to be measured when calculating the insulation resistance and the current is measured. This voltage and current ratio gives us the insulation resistance [22].

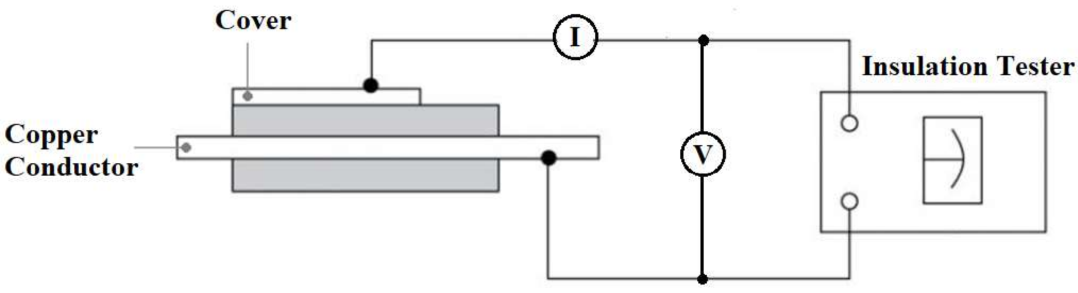

Figure 2.2 Insulation tester connection diagram [22]

2.4 Insulation Test Methods

2.4.1 Dielectric Isolation Power Test

This is also called endurance test. A voltage value above the maximum use voltage of the conductor is applied for a specified period of time. The applied voltage, the rate of application and the duration of the test depend on the specification requirements of the conductor or equipment under test. The conductor under test must withstand the applied voltage during the test period [23].

The dielectric strength test is applied as follows; [23, 25]

- The working voltage or higher voltage given in the specification of the equipment or cable is applied between the isolated lines or between the isolated lines and the ground.
- After the applied voltage reaches equilibrium (steady-state), leakage current measurement is made between the relevant lines for the specified time (dwell time). If the leakage current limit is exceeded at any time during the measurement process, the test fails.
- Performing the test on a faulty conductor assembly may result in permanent damage or sudden discharge. Typical hipot equipment leakage current trip limit settings vary from 0.1 to 20 mA and are adjusted by the user according to test object characteristics and voltage application speed. The goal is to select a current setting that will not cause the tester to turn on incorrectly during voltage application, while also selecting a value that minimizes potential damage to the tested device or cable when accidental discharge or malfunction occurs.
- If the leakage current limit is not exceeded during the measurement process, the test is completed successfully.

Dielectric strength is tested with high voltage source, voltage and current meters. However, "hipot tester" is generally used to perform this test. This device applies the required voltages to the equipment or cable under test and monitors leakage current [23].

2.4.2 High Voltage Isolation Test

The insulation resistance test is applied to determine whether the insulation resistance value between the split lines in the cable harness is ideal or sufficient under daily environmental conditions. By the insulation resistance measurement, the conditions such as wear, deterioration and loss in the insulation material resulting from environmental factors such as heat, moisture, dirt can be determined, as well as the determination of moisture (after sealing) on the spacers [24].

The insulation resistance test is applied as follows; [24,25]

- A certain constant voltage is applied between the isolated lines or between the isolated lines and ground (taking into account the voltage and possible instantaneous voltage jumps to which the harness will be exposed in use).
- A certain time (soak time) is expected for the system to stabilize. Leakage current changes during this time (soak time) are ignored.
- After the soak time, leakage current is measured during the test period. Insulation resistance is calculated by the ratio of applied voltage to leakage current ($R_{ins} = V_{ir} / I_{leak}$).
- If the measured insulation resistance is greater than the previously determined insulation resistance, the test is successful; however, the test fails, if it is small.

Insulation resistance test can be done with cable tester or megaohmmeter with sufficient voltage and resistance measurement capacity [24].

2.4.3 Step Voltage Test

Voltage is gradually increased in step voltage test. While a good insulating material shows constant resistance at different voltage values, the insulation resistance of bad insulating material decreases as the voltage increases [26].

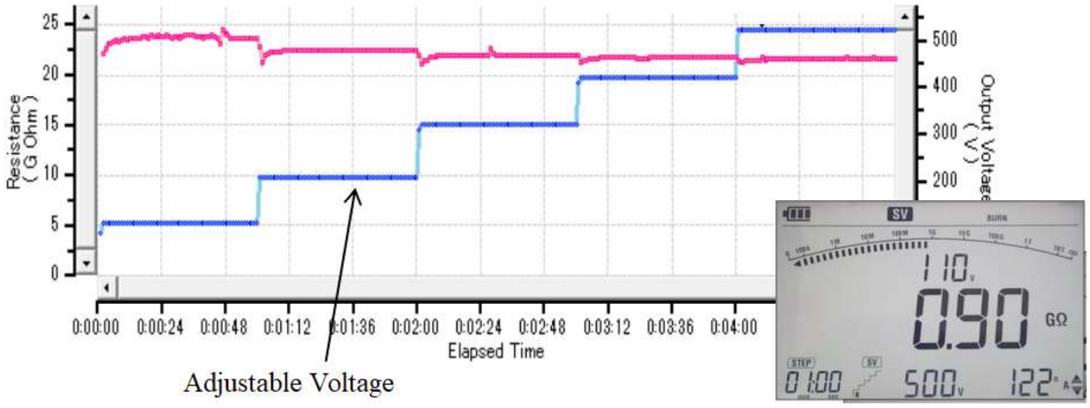

Figure 2.3 Step voltage test graph [26]

2.4.4 Ramp Test

This test method has two different measuring modes. The first one is the breakdown mode. In this mode, a voltage that is as rising as the selected voltage in the ramp test is produced. A sudden current increase is detected and the applied voltage drops when a distortion occurs. The measurement is automatically terminated so that the tested object is not damaged. The measurement does not stop without a sudden increase in current [26].

Mode 2 is the burn mode. The measurement does not stop even if a sudden current increase is determined. It is a method used to determine the damage at the point of failure and to locate the point of failure [26].

2.4.5 Polarization Index

Polarization index shows the effect of time om the measurement of insulation resistance. So it is the process of saturating the conductor. The ratio of the high voltage applied to the conductor to the insulation resistance at the end of 3 - 10 minutes and the insulation resistance at the end of 30 - 60 seconds indicates the polarization index. Table 2.3 shows the classification of the conductor insulation according to the value obtained [26].

Table 2.3 Polarization status table [26]

Polarization Index	4.0 and above	4.0 - 2.0	2.0 - 1.0	1.0 and below
	very good	good	suspicious	Bad

CHAPTER 3

ISOLATION TEST SYSTEM DESIGN

3.1 Rectifier Circuit and Input Capacitor Calculation

The driver circuit of the cable test system is built with SMPS (Switch Mode Power Supply) circuit logic. Therefore, rectification circuit and input capacitors are calculated according to H-Bridge topology.

Figure 3.1 shows the schematic of the rectifier circuit. In order to prevent sudden charging of the rectifier capacitors, a relay ntc circuit has been installed. When the system is first energized, the input capacitors are charged with limited current through NTC. After 1 second, the relay is triggered and NTC is deactivated. In order to reduce the internal resistance (ESR) of the input capacitors in the circuit, smaller capacitors are paralleled instead of a single large capacity capacitor [27].

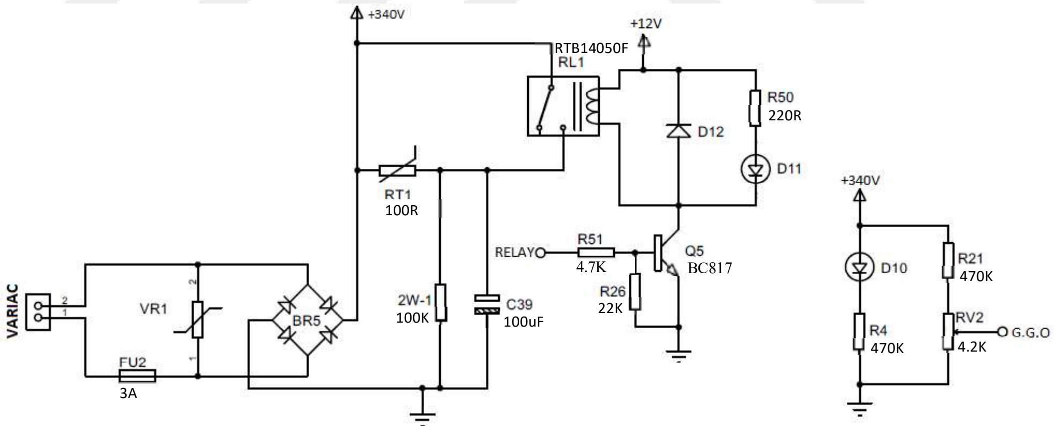

Figure 3.1 Rectifier Circuit

Acceptable oscillation value (ΔV), when AC voltage from auto transformer is converted to DC voltage after rectification, is taken as 1% of nominal voltage value. Accordingly, the capacitor value that should be put into operation is calculated below. In addition, the frequency value of the high voltage transformer was calculated according to the value read from the input voltage. The input voltage is calculated by the voltage divider circuit connected to the DC bus voltage. The value obtained here is input voltage found connecting ADC reading pin [27].

$$Q = C \times V \quad \textbf{(3.1)}$$

$$Q = I \times T \quad \textbf{(3.2)}$$

$$I \times T = C \times \Delta V, \quad \Delta V = V_{p-p} \quad \textbf{(3.3)}$$

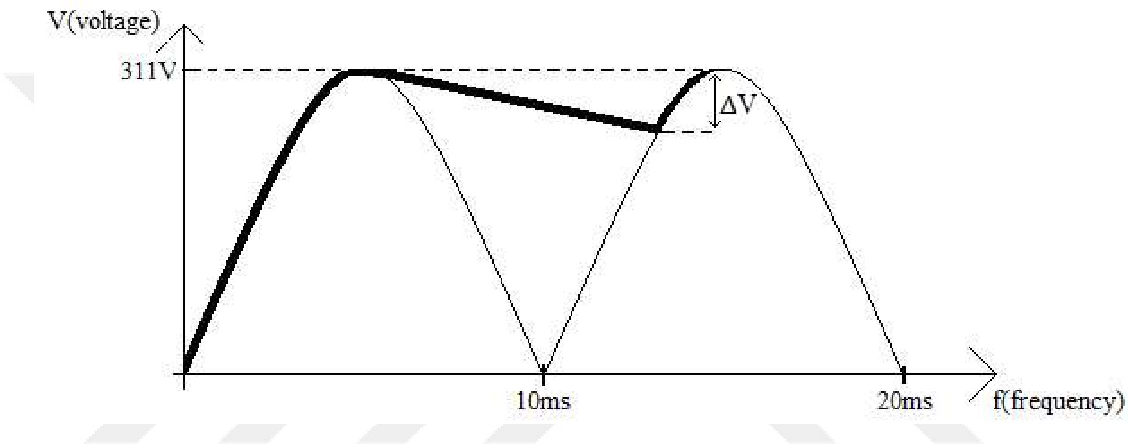

Figure 3.2 Rectifier circuit V/f graph

In practice, the ΔV value is taken as 1% of the DC bus voltage.

$$C = I \times \frac{T}{\Delta V} \quad \textbf{(3.4)}$$

$$C_{in} = 1 \times \frac{10 \times 10^{-3}}{3.11} = 3215\ \mu F \quad \textbf{(3.5)}$$

3.2 High Frequency Transformer Design

The drive circuit of the cable test system is designed grounding on the H-Bridge SMPS circuit. Therefore, calculations of the high frequency transformer were made based on the H-Bridge SMPS topology. In addition, the selection of the conductor to be used for transformer selection is of great importance. So, conductive wire must be calculated first to be used will be done first.

3.2.1 Calculation of Primary and Secondary Wire Sections

Skin effect is a significant problem in conductors which carried high frequency signals. Skin effect can be briefly explained as follows; electromotive forces are induced in the conductor due to the constantly changing direction of the magnetic field in the conductor. These create circular currents in the conductor. In the literature, these currents are called eddy currents (Eddy-Foucault). These currents are shown in Figure 3.3. The eddy currents push the current passing through the conductor towards the outer wall of the wire. In this case, no current flows through the center of the wire. As the frequency increases, the area that does not pass current grows [27, 28].

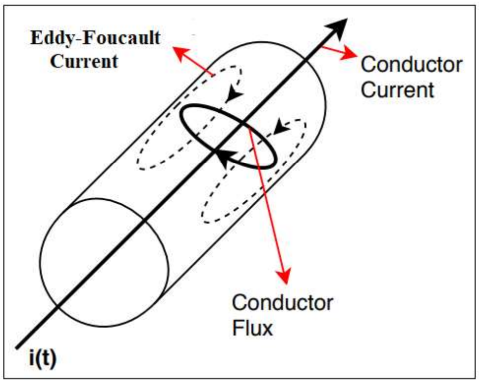

Figure 3.3 Eddy-Foucault current in a solid conductor [27]

The skin effect calculation is shown in Equation 3.6. The value obtained here refers to the thickness of the diameter through which the current passing through the conductor will flow at the calculated frequency value. In other words, the conductor to be selected must be selected smaller than this value.

$$\delta = \sqrt{\frac{\rho}{f\ x\ \pi\ x\ \mu}} = \sqrt{\frac{1.724\ x\ 10^{-8}}{5000\ x\ 3.14\ x\ 4\ x\ 3.14\ x\ 10^{-7}}} = 0.93\ mm \quad \textbf{(3.6)}$$

The wire to be used in line with the value obtained from Equation 3.6 should be chosen smaller than the Skin Effect depth. The 0.5 mm^2 conductor should be used. Since our current going through the primer is a small value such as 1 ampere, it is sufficient to use a single conductor in the transformer. Since our secondary current will be much smaller than the current passing through the primary, we also need to choose the secondary conductor thinner since the number of turns to be wrapped in the secondary is very high. Since the current that will pass through the secondary winding will be 20 times smaller due to the primary current of the transformer winding ratio, and the current that will pass through the primary winding will be maximum 1 A. The maximum current that will pass through the secondary winding is $\mathbf{I_{sec}}$= 1/20 = 50 mA. Accordingly, 0.03mm^2 wire is suitable for our secondary winding [27, 28].

3.2.2 Calculation of Primary and Secondary Winding Numbers

The percentage of power switches remaining on during a duty cycle must first be calculated. Due to the structure of H-Bridge switching, cross switch pairs (H1 / L2 - H2 / L1) are switched respectively. Although there is no dead time (t_{dt}) left between these switch pairs in theory, the dead time should be left a little more than the sum of the switches entering and transmitting in practical time. In this study, dead time is determined as 10 $\boldsymbol{\mu}$s with the help of processor. The period duration was calculated in equation (3.7) to find out how much of the determined dead time affects 1 duty cycle [27].

$$T = \frac{1}{f_s} = \frac{1}{5000} = 200\ \boldsymbol{\mu} s \qquad \textbf{(3.7)}$$

The specified dead time is equal to $\frac{(5\ \mu s + 5\ \mu s)}{200\ \mu s}$ x 100 = 5%. Within the period duration and dead time determined, the working percentage (duty) of a switch pair is calculated in the equation (3.8) [27].

$$D = (100\% - 10\%) / 2 = 45\% \qquad \textbf{(3.8)}$$

One of the significant points to be considered while winding calculation of the transformer is copper and core losses. If the number of turns is more than it should be, core losses will decrease but copper losses will increase excessively. Otherwise, copper losses will decrease while core losses will increase. Figure 3.4 shows the relationship between two losses [27, 29].

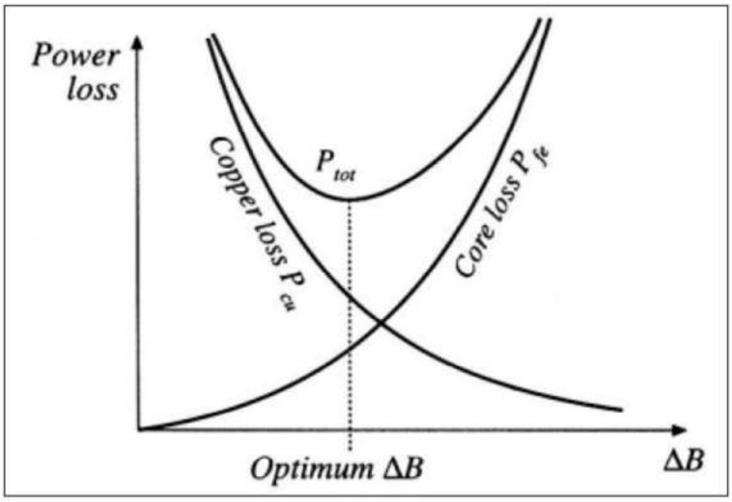

Figure 3.4 The relationship between copper and iron losses on the transformer [28]

Here, ΔB value represents the magnetic flux density when the transformer is operating at full load from no-load value. The B-H curve given in the technical document of the material from which the magnetic core is made is given in Figure 3.5. Referring to Figure 3.5, the B_{max} value is taken as 0.35 T. Since the ΔB value exceeds this value, the magnetic core is saturated. Also, the closer the ΔB value is to the B_{max} value, the more the magnetic core will get warmer. Therefore, ΔB = 0.25 T [27].

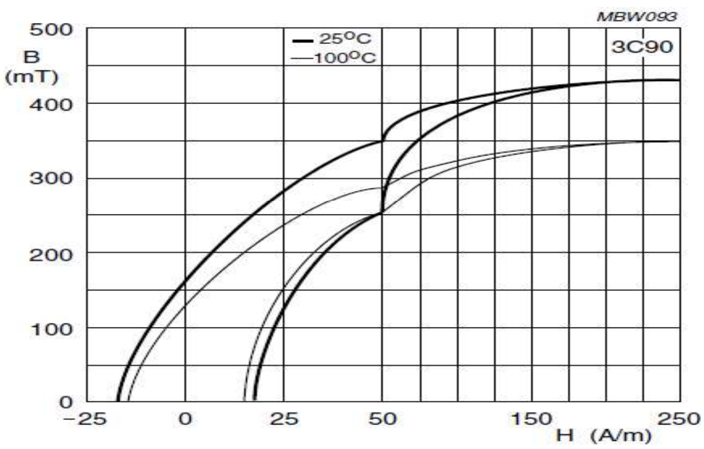

Figure 3.5 B-H curve of 3C90 material

AC signal applied to the primacy was used to calculate primary winding. Figure 3.6 shows the AC signal applied to the primer. Here, λ represents the shaded area [27,29].

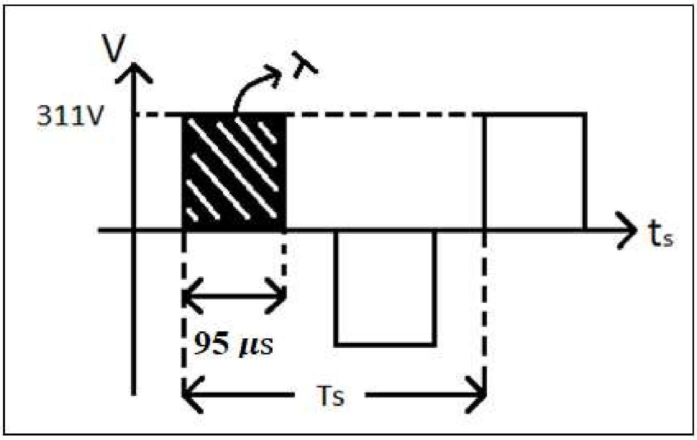

Figure 3.6 AC voltage applied to the primary winding

λ value is calculated below, ΔB value is selected as 0,25 T and A_e value is taken from the technical document of the core. In accordance with these values, the number of primary windings was calculated by equation (3.9) [27, 29].

$$\lambda = \int_{t1}^{t2} V_1(t)\, dt \tag{3.9}$$

The change of the voltage induced over a coil over time causes a change in the flux density (B). Therefore, the change of flux density according to Faraday's law;

$$\frac{dB(t)}{dt} = \frac{V}{N\,x\,A_e}\,x\,D\,x\,T_s \tag{3.10}$$

$$\lambda = V\,x\,D\,x\,T_s/2 \tag{3.11}$$

$$\Delta B = \frac{\lambda}{2\,x\,N\,x\,A_e} \tag{3.12}$$

If we calculate the number of N_s windings from Equation (3.12);

$$N_s = \frac{\lambda}{2\ x\ \Delta B\ x\ A_e} \qquad \textbf{(3.13)}$$

$$\lambda = 311\ V\ x\ 95\ x\ 10^{-6} = 29.54\ mV.\ s \qquad \textbf{(3.14)}$$

$$N_P \ = \frac{29.54\ x\ 10^{-3}}{2\ x\ 0.25\ x\ 683\ x\ 10^{-6}} \approx 86\ turns \qquad \textbf{(3.15)}$$

After the primary winding was calculated, the secondary winding number was calculated by equation (3.16).

$$N_S = \frac{1}{2\ x\ D}\ x\ N_P\ x\ \frac{V_{out}}{V_{in}} = \frac{1}{2\ x\ 0.45}\ x\ 86\ x\ \frac{5000}{311} \approx 1536\ turns \qquad \textbf{(3.16)}$$

3.2.3 Transformer Carcass Design

Transformer design was made as in Figure 3.7 first. In this way, it was intended to avoid this situation, since a voltage greater than its capacity is induced on the secondary conductor. There are 291 rounds in each section. In this way, only 1000 V voltage will be induced in each section. However, since this carcass design increased the stray capacitance on the transformer, it caused overvoltage oscillations on the secondary voltage. Therefore, the classical carcass design was preferred, with the primary voltage inside and the secondary voltage outside.

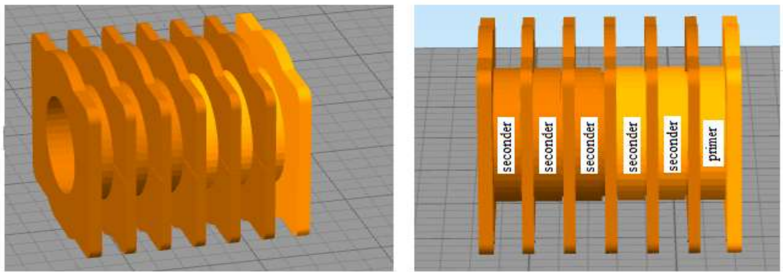

Figure 3.7 HFT carcass design

3.3 Design of MOSFET Driver and Control Circuit

While driving the power switches used in H-Bridge drives, three electrically isolated separate sources are required as per topology. Although the reference points of the two bottom MOSFETs are the same, a separate riding source is required for each of the upper arm MOSFETs. MOSFET drivers used at this point must also be insulated drivers. Also, keeping the reference point of the control card and the reference points of the MOSFETs apart is of great importance for the system to work more stable and to prevent the noise caused by switching from affecting the control card. Therefore, four separate isolated sources are used in the system. Gate ends of MOSFETs are driven with a high voltage that the processor cannot provide. Considering the technical document of MOSFET with code 7NM70G used in this circuit, it was found that the maximum voltage that can be applied is 30 V. Four independent sources were obtained using 2 of the 50 Hz transformers with a power of 3.5 VA, 15 V (AC), which can provide 2 separate outputs for the isolated source in the circuit. A voltage of 15 V (AC) was rectified by a bridge diode and capacitor and applied to the supply of the HCLP3120 coded MOSFET driver, which is a totempol structure, as 18 V. One of the points to be considered here is the threshold voltage of the MOSFET driver. If a voltage is applied below the threshold voltage of the MOSFET driver, MOSFET will not be driven, even if the applied voltage is sufficient to drive the MOSFET gate, since the driver cannot exceed the threshold voltage. Looking at the worksheet in the technical document of the HCLP3120, it has been seen that the minimum voltage to be applied to the MOSFET driver is 13.5 V. However, to charge the gate capacitors in MOSFETs more quickly and put the MOSFET into a faster transmission, applying higher voltage than the threshold voltage is an important detail in driving MOSFET. Otherwise, since the MOSFETs will open and close later, the dead time left between the cross-driven MOSFETs may be insufficient and cause a conflict, causing MOSFETs to short circuit. Also, since this will maximize switching losses, both the loss in the circuit will be more and the heating on the switches will be more than necessary [27].

Looking how much current the processer would draw may be the first thing to do when calculating the power expenditures in the control circuit. Figure 3.7 depicts the table showing the electrical characteristics of the processor with the code DSPIC33FJ64MC204 selected for this design. The MIPS value given here shows the amount of command that the processor processes per second. Although the operating frequency and MIPS values are not the same, it can be selected from the table according to the MIPS value because they are related to each other [27].

Table 3.1 MCU MIPS current table

DC CHARACTERISTICS			Standard Operating Conditions: 3.0V to 3.6V (unless otherwise stated) Operating temperature -40°C ≤ TA ≤ + 85°C for Industrial -40°C ≤ TA ≤ +125°C for Extended			
Parameter No.	Typical(1)	Max	Units	Conditions		
Operating Current (IDD)(2)						
DC20d	19	30	mA	-40°C	3.3V	10 MIPS
DC20a	19	30	mA	+25°C		
DC20b	19	30	mA	+85°C		
DC20c	19	35	mA	+125°C		
DC21d	29	40	mA	-40°C	3.3V	16 MIPS
DC21a	29	40	mA	+25°C		
DC21b	28	45	mA	+85°C		
DC21c	28	45	mA	+125°C		
DC22d	33	50	mA	-40°C	3.3V	20 MIPS
DC22a	33	50	mA	+25°C		
DC22b	33	55	mA	+85°C		
DC22c	33	55	mA	+125°C		
DC23d	47	70	mA	-40°C	3.3V	30 MIPS
DC23a	48	70	mA	+25°C		
DC23b	48	70	mA	+85°C		
DC23c	48	70	mA	+125°C		
DC24d	60	90	mA	-40°C	3.3V	40 MIPS
DC24a	60	90	mA	+25°C		
DC24b	60	90	mA	+85°C		
DC24c	60	90	mA	+125°C		

Considering the table in Table 3.1, the DC24a parameter is taken as reference because the processor's operating frequency is selected as 40 Mhz. Accordingly, the current drawn by the processor is determined as 60mA. Due to the fact that linear regulators are used to reduce the 18 V transmitted from the transformer to the processor voltage, the power calculation according to the DC output voltage given by the transformer is shown in the equation (3.17), while the power consumption spent by the processor is not calculated according to the processor voltage of 3.3 V made like [27].

$$P_{proccessor} = 18\ V\ x\ I_{proccessor} = 18\ V\ x\ 0.06\ A = 1.08W \quad \textbf{(3.17)}$$

Another element power consuming is the LCD. The power drawn by the LCD was measured as 20 mA with the help of a power source. Accordingly, the power consumed by the LCD is calculated in the equation (3.18) [27].

$$P_{LCD} = 18\ V\ x\ I_{LCD} = 18\ V\ x\ 0.02 = 0.36W \quad \textbf{(3.18)}$$

The total power drawn by the control board is 1.08W + 0.36W = 1.44W. Since the power of a single channel of the 3.5W transformer makes 1.75W, it can provide the power of the control card. Figure 3.8 shows the drawing of the control circuit [27].

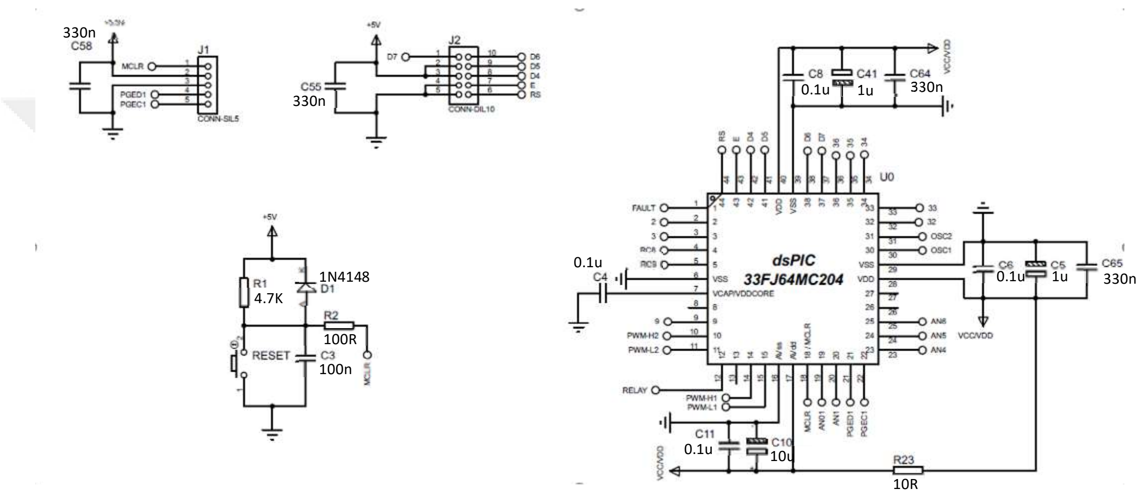

Figure 3.8 Control circuit of system

Figure 3.8 shows the processor, LCD connection, programming tips, reset circuit and current reading circuits. The switching of the MOSFETs in the power circuit is controlled by the processor's Motor Control PWM Module (MCPWM). Current reading was done with Shunt resistors via INA200 integration.According to the current passing through the resistors, the value read from the out pin of the integrated device was entered into the processor and current control of the system was performed.

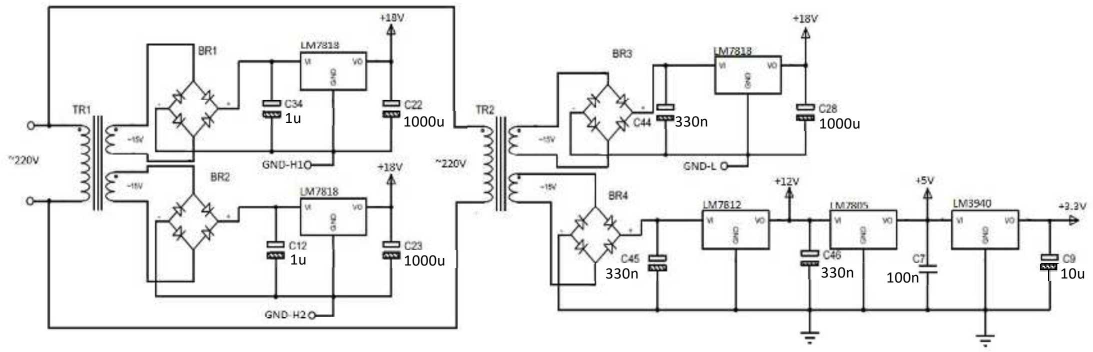

Figure 3.9 Supply of control circuit and MOSFET driver

Figure 3.9 shows the insulated feeding circuit. The outputs of the 0.5 VA transformer used to drive the upper arm MOSFETs are rectified with a bridge diode and capacitor, fixed to 18 V with the LM7818 regulator and gave to the feeding of the MOSFET drivers. It should be noted here that the signal reference terminal of the MOSFET drivers and the reference terminals of the MOSFET are kept separate. Figure 3.10, shows the MOSFET driver circuit.

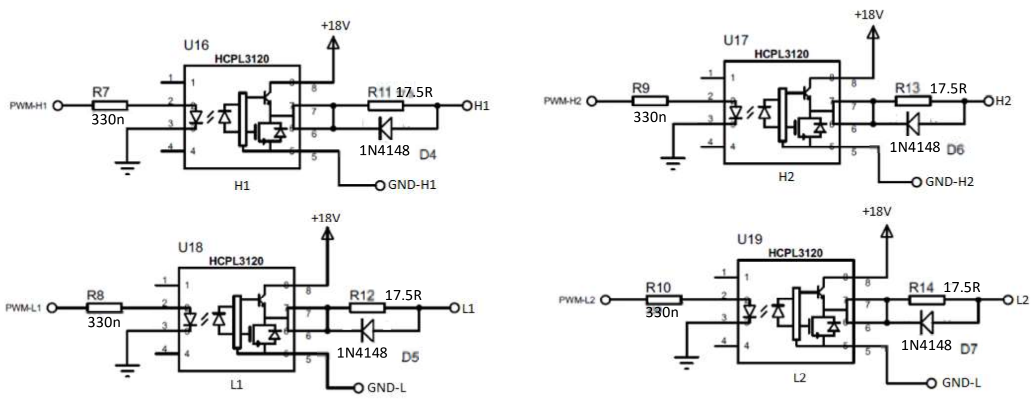

Figure 3.10 MOSFET driver circuit

One of the significant points in insulated MOSFET driver circuits is that the processor reference and MOSFET's reference ends must not be the same. In addition, in order to allow MOSFET to go to the fast cutting, a fast diode was placed parallel to the driving resistance and inverted for the fast discharge of the Gate-Source capacitor. Then, equation (3.19) was used to calculate the I_{GS} current.

$$I_{GS} = C_{iss}\ x\ \frac{\Delta V}{\Delta t} \tag{3.19}$$

Here ΔV = V_{GS}, and Δt is the opening time of MOSFET. C_{iss} = 400 pF and this value is taken from the technical document of MOSFET. I_{GS} value was calculated by replacing these values.

$$I_{GS} = 400\ x\ 10^{-12}\ x\ \frac{18}{100\ x\ 10^{-9}} = 0.072$$

The driving resistance of MOSFETs was calculated by substituting the I_{GS}value in the equation (3.20).

$$R_{GS} = \frac{V_{GS}}{I_{GS}} \tag{3.20}$$

$$R_{GS} = \frac{18}{0.072} = 250\ \Omega \tag{3.21}$$

3.4 Power Switch Selection and H-Bridge Structure

The main task of the power switches is to convert the DC voltage to high frequency AC voltage with the PWM signal controlled from the processor, using the rectified mains voltage. Circuit parameters (current, voltage, frequency, power) should be considered when selecting power switches. Since the current value transferred in this system is quite low, a switch with low current capacity has been selected. As a switch, SMD MOSFETs with 7NM70G-TN3-R code belonging to UTC Company were preferred. The drain-source voltage of the MOSFETs used in the power circuit is 700 V and the R_{ds} resistance is less than 1 Ω. Since the DC bus voltage applied to the power circuit is 310 V and the stresses occurring between drain-source during the switching can reach up to 600 V, MOSFET with a strength above this value is preferred.

In this thesis, the H-Bridge switching circuit shown in Figure 3.11 is used to switch the high frequency transformer used to increase the voltage. With the current reading circuit placed between the power circuit and the negative polarity of the DC bus, it is understood that at what voltage level the conductor of the tested conductor began to be pierced. In addition, RCD Buffer Snubber Circuit was applied to the power circuit in order to reduce stresses on the switch.

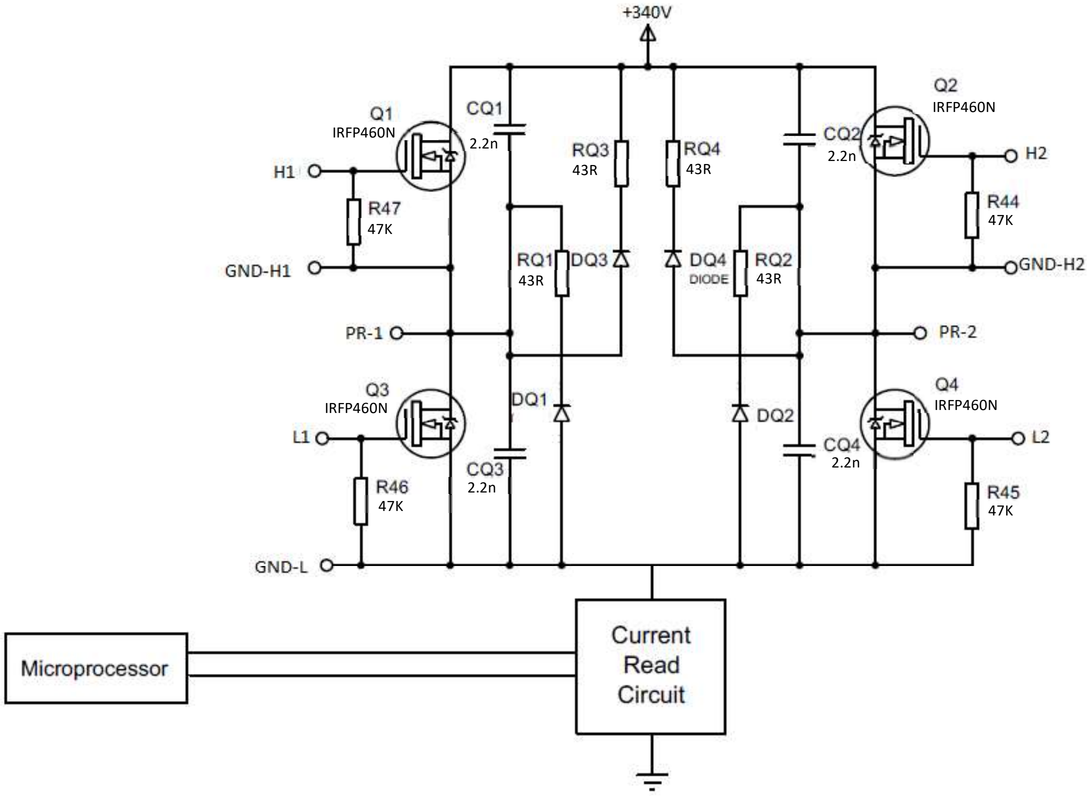

Figure 3.11 H-Bridge switching circuit

3.5 Current Reading Circuit

The current reading power circuit is created with shunt resistors located between the Source end of the lower arm switches and the negative polarity of the power circuit. Considering the operation logic, the current begins to pass when puncture begins on the test lead connected to the secondary end of the high frequency transformer. 20 times more of the current passing through the secondary simultaneously (since the winding ratio is 20) starts to flow through the primary winding. As seen in Figure 3.12, the current passing through the primary winding flows to the ground through the shunt resistors.

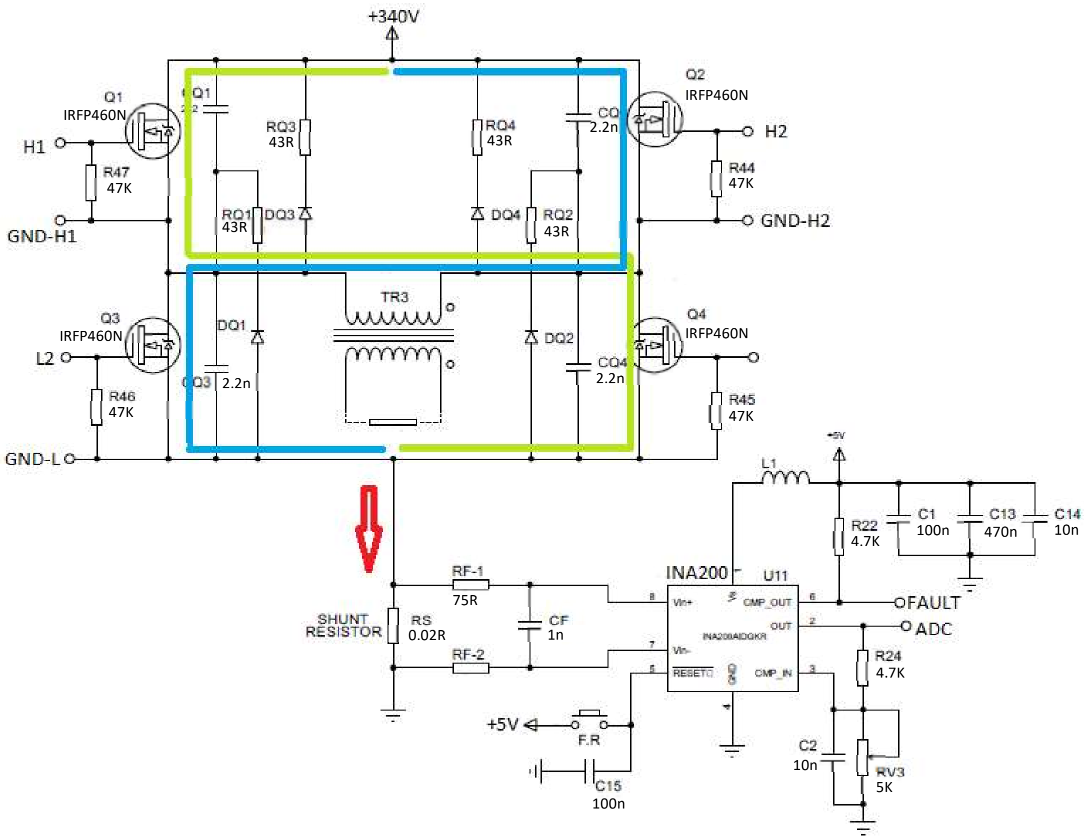

Figure 3.12 Current reading circuit and connection with power circuit

Here, the voltage created by the current passing through the shunt resistors is amplified with the amplifier OP-AMP, and then output is obtained when the current value is exceeded with an OP-AMP which performs comparison. For this process, INA200AIDGKR integration belonging to Texas Instruments Company was used. Figure 3.13 shows the internal structure of the integrated. As can be seen from here, there are two OP-AMPs inside the integrated. Of these, the OP-AMPS connected to pin 7 and 8 work as a discriminator and strengthen the voltage entering these pins 20 times. The amplified voltage value is entered into the inverting end of the receiver OP-AMP and compared with the integrated reference voltage of the integrated. CMP_{out} pin becomes active when the voltage value determined according to the value of the shunt resistance exceeds the internal voltage value in the comparison OP-AMP. This pin was reversed with a reverser or a transistor and entered into the FAULT pin of the processor. Generally, the processors understand the error by pulling the error pin from the pin voltage to 0 V, or otherwise; they cannot check if the system is working. Also, the integrated goes into a permanent state when the CMP_{out} pin is active. In order to reset this pin, RESET pin number 5 of the integrated must be set to 0 V.

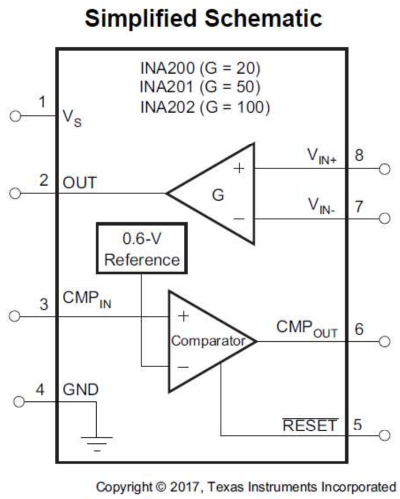

Figure 3.13 Internal structure of the INA200AIDGKR integrated

3.6 High Voltage Reading Circuit

The high voltage reading circuit is designed to perform reading from the secondary end of the high frequency transformer. Instead of a conventional voltage divider and rectifier diodes, the voltage divider and Full Wave Precision Rectifier circuit are installed together. Otherwise, the high voltage reading process cannot be performed precisely and linearly due to the voltage falling on the rectifier diodes. The Full Wave Precision Rectifier circuit consists of a combination of voltage tracker (U1: A) and inverting amplifier (U1: B) circuits. Rectifying is done with diodes again. Since the output of U1: A will be positive in the positive alternance of the input voltage, D1, which is the correct polarity, becomes a short circuit by going to the transmission, while D2 is an open circuit by going to the cut. U1: A and U1: B both acts as voltage monitors. Therefore, in positive alternances, the output voltage is equal to the input voltage. Since the output of U1: A will be negative in the negative alternance of the input voltage, D1, which is the reverse polarity, goes to the cut and becomes open circuit, and D2 goes to the transmission and shows a short circuit feature.U1:A OP-AMP acts as a voltage follower, while U1:B acts as an amplifier inverting the OP-AMP. In this circuit, R1 and R3 resistors are selected equally. U1: Output B has the same input signal and this signal is applied to the amplifier none inverting over the R1 resistor. Thus, negative alternances of the input voltage are transferred to the output by changing the phase 180°. Figure 3.14 shows the input and output voltage graphs of the Full Wave Precision Rectifier circuit.

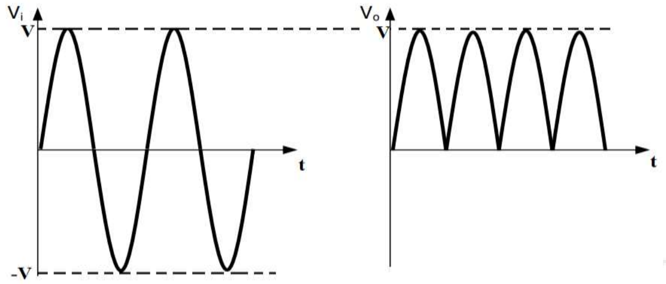

Figure 3.14 Input and output signals of the high voltage rectification circuit

Figure 3.15 shows the schematic of the high voltage reading circuit. The ratio of the voltage divider is set to 1000:1. Thus, after rectifying operation, it is possible to read directly from the processor's ADC pin without the need for a voltage divider again.

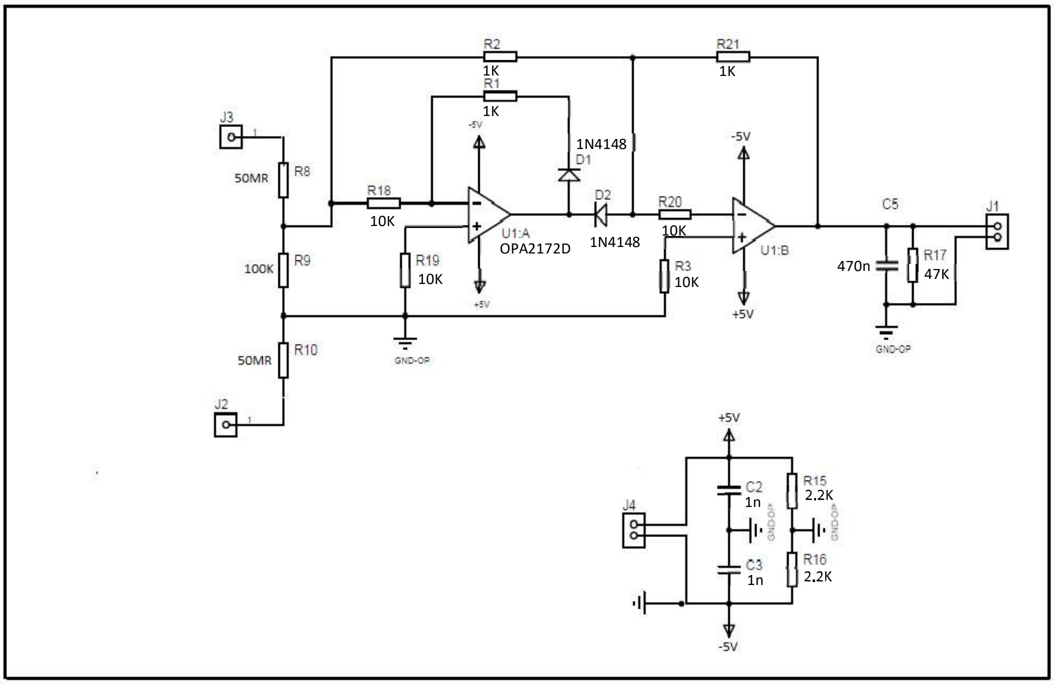

Figure 3.15 High voltage sense circuit

OPA2172 integration of Texas Instrument Company, which contains two OP-AMPs, was used for a sensitive reading process. Both positive (+12 V) and negative (-12 V) voltages are applied to the OP-AMP feeds so that the OP-AMPs can be corrected at the sign in the negative cycle.

3.7 Snubber Circuit

MOSFETs, which are used as power switches in full bridge DC-DC converters, are exposed to a rapid current rise (di / dt) at the time of transmission and a rapid voltage rise (dv / dt) at the time of cutting. In this case, snubber circuits are used to prevent allowed current and voltage spikes. Snubber circuits have 3 different purposes. The first method is Turn-Off Snubber Circuit. The purpose of the Turn-Off Snubber Circuit is to provide a voltage close to zero at the switch ends until the switch current reaches zero. Turn-On Snubber Circuit is used to decrease the di/dt ratio of the switch during the transmission. The Overvoltage Snubber Circuit is used to prevent overvoltage at the switch ends due to the stray inductances during switch cutting. The snubber circuit used in this circuit is the Turnoff Snubber Circuit. The diagram of the Snubber Circuit used for Full Bridge DC-DC Converter is shown in Figure 3.16 [28].

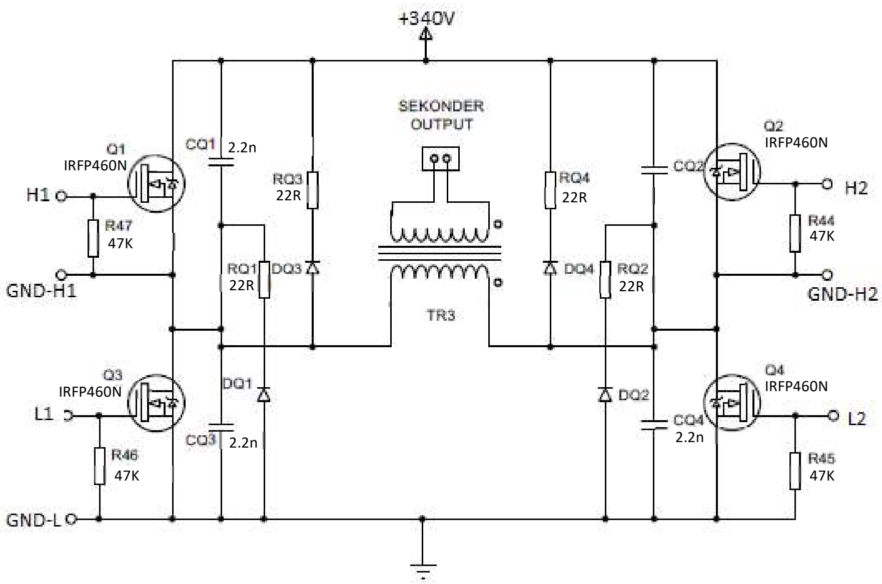

Figure 3.16 RCD Buffer Snubber Circuit for Full-Bridge Topology

Unlike other RCD snubber circuits, the RCD Buffer Snubber circuit regains the stresses it receives from the switches over a resistor instead of spending it on a resistor. If we examine the working principle; considering that the Q1 switch is in the cut and the Q3 switch is in transmission, the stress on the Q1 switch is absorbed into the CQ1 capacitor via the Q3 switch as seen in Figure 3.17 (a). With the entry of switch Q3 into the cut, some of the energy stored on CQ1 is fed back, while the other part is spent on RQ1 resistance. This situation is as seen in Figure 3.17 (b) [30].

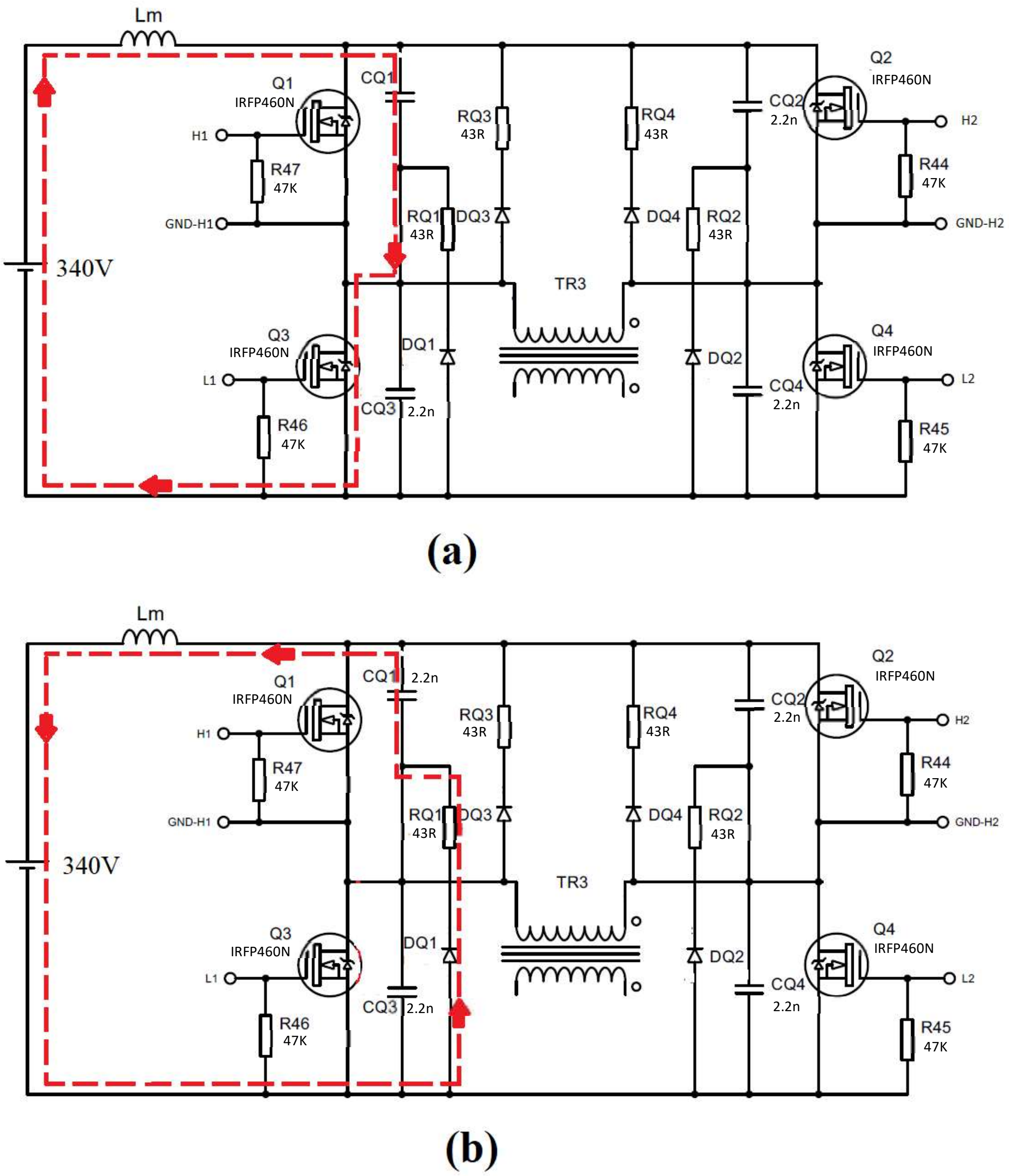

Figure 3.17 Operating principle of the RCD Buffer Snubber Circuit for switch Q1

The parameters of the RCD Buffer Snubber Circuit with the Q1 switch are calculated below.

$$CQ_1 = \frac{L_m \; x \; I_d^2}{\Delta U\% \; x \; V_{dc}} \tag{3.22}$$

$$\sqrt{\frac{L_m}{CQ_1}} \leq RQ_1 \leq \frac{1}{2 \; x \; 3 \; x \; CQ_1 \; x \; f_s} \tag{3.23}$$

$$P_{RQ_1} = \frac{1}{2} \; x \; L_m \; x \; I_d^2 \; x \; f_s \tag{3.24}$$

In the equations given above, ΔU value represents the voltage fluctuation value and is taken as 20% in this system. f_s Value is the switching frequency of the system and it is taken as 5 kHz L_m value is the parasitic inductance value of the system and this value is the inductance value that is read from the primary after the secondary of the transformer is short-circuited. In the light of these values, the resistance and capacitor values that should be installed in the system are calculated below.

$$CQ_1 = \frac{1.12 \; x \; 10^{-3} \; x \; 0.5^2}{(20\% \; x \; 340)^2} = 60.5 \; nF \tag{3.25}$$

Since the value obtained from Equation (3.25) is not a market value, it is preferred to use 47 nF as the closest available value. Resistance value of RCD Buffer Snubber Circuit were calculated by equation (3.26)

$$\sqrt{\frac{1.12 \; x \; 10^{-3}}{47 \; x \; 10^{-9}}} \leq RQ_1 \leq \frac{1}{2 \; x \; 3 \; x \; 47 \; x \; 10^{-9} \; x \; 5000} \tag{3.26}$$

$$154 \leq RQ_1 \leq 709 \tag{3.27}$$

The resistance value of the snubber circuit was chosen as 220 R (ohms) according to this calculated value. With the equation (3.28), the power value to be spent on the resistance also calculated.

$$P_{RQ_1} = \frac{1}{2} \; x \; 1.12 \; x \; 10^{-3} \; x \; 0.5^2 \; x \; 5000 = 0.7 \; W \tag{3.28}$$

CHAPTER 4

EXPERIMENTAL STUDIES

4.1 System and PCB Design

Figure 4.1 shows the test scheme of the H-Bridge switched highvoltage test circuit prepared in the laboratory.

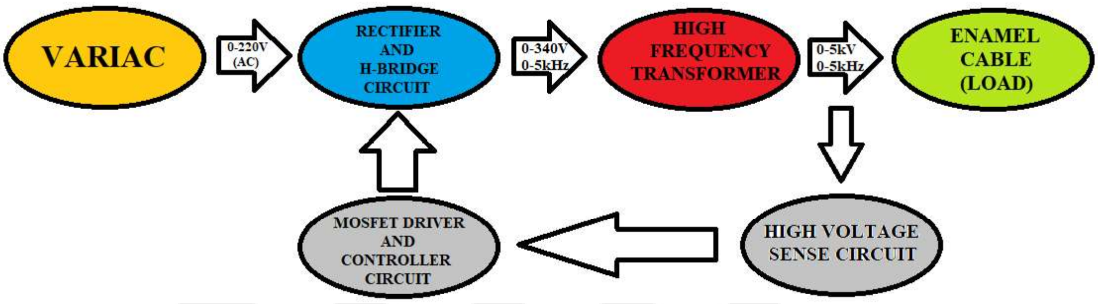

Figure 4.1 System test schematics

The PCB design is designed reciprocally in Proteus program. The PCB measures 16.5 x 7.6 cm. The top and bottom view of the PCB drawing is given in Figure 4.2 and Figure 4.3 respectively.

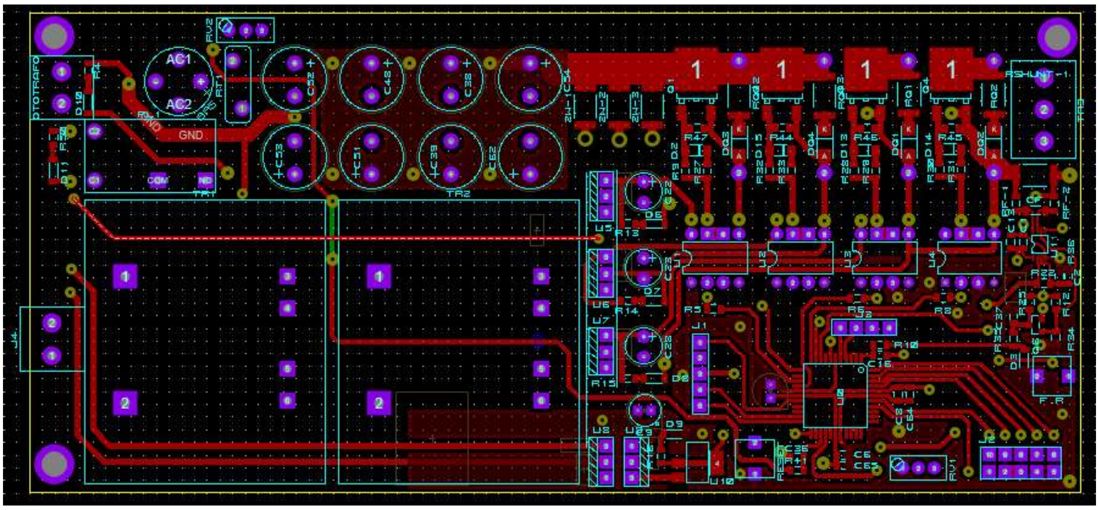

Figure 4.2 Top silk and top copper of PCB

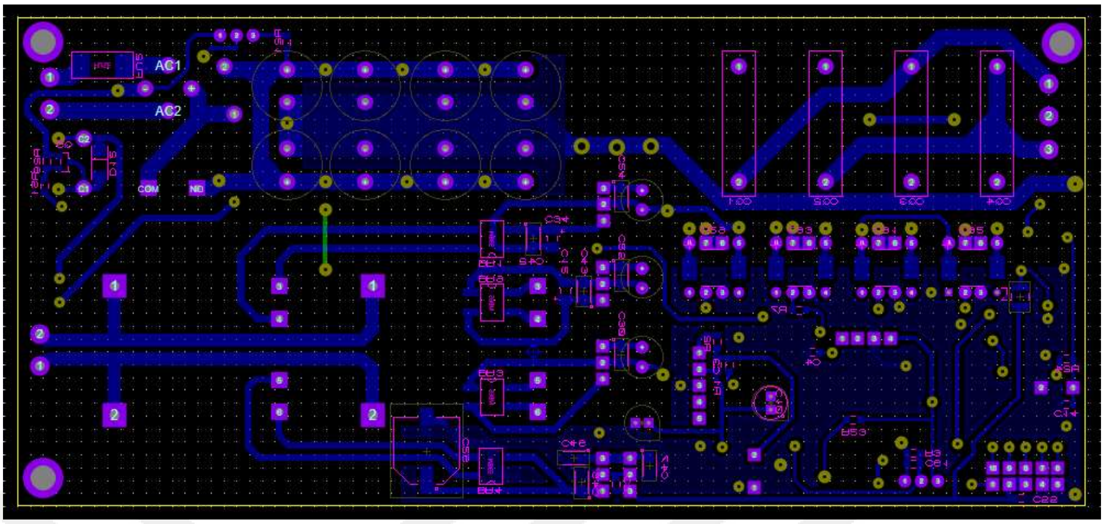

Figure 4.3 Bottom silk and bottom copper of PCB

4.2 MOSFET Switching Forms

Since the basic structure of the system is H-Bridge, the power switches are designed to be cross, that is, Q1-Q4 and Q2-Q3 key pairs are at the same time in transmission and cutting. If the Q1-Q3 and Q2-Q4 key pairs are transmitted at the same time, the system will be short-circuited, so a dead time is left between these key pairs with the help of a microprocessor. Figure 4.4 shows MOSFET switching forms. Channel 1,2,3 and 4of the oscilloscope here represent the trigger signals for MOSFETs Q1 (H1), Q2 (H2), Q3 (L1) and Q4 (L2) , respectively. The oscilloscope image was taken when the system was at the highest frequency. It is seen that the dead time between the upper and lower MOSFETs is set to 10 μs with the help of the processor.

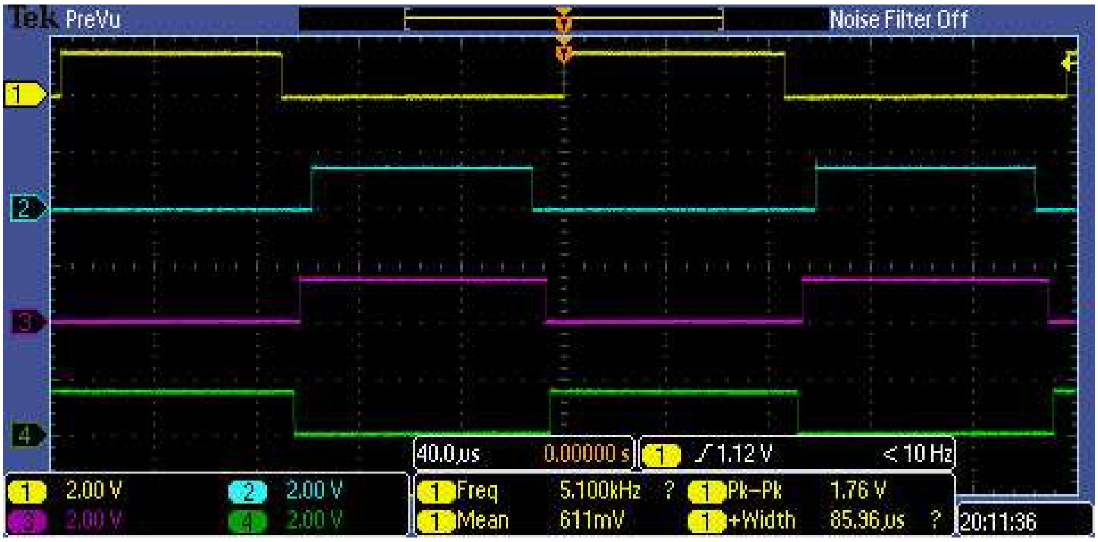

Figure 4.4 H-Bridge switching form

4.3 Experimental Setup and Results

The test setup of the enamelled cable test system with H-Bridge driver is as shown in Figure 4.5. The 0-220 V AC voltage received from variac is rectified and creates the DC bus voltage of the H-Bridge circuit. The control of variac is provided by controlling the 12V DC motor on variac with a DC motor driver circuit. Control of DC bus voltage is provided by controlling variac. Thus, the amplitude value of the AC square wave signal created by the H-Bridge circuit can be adjusted.

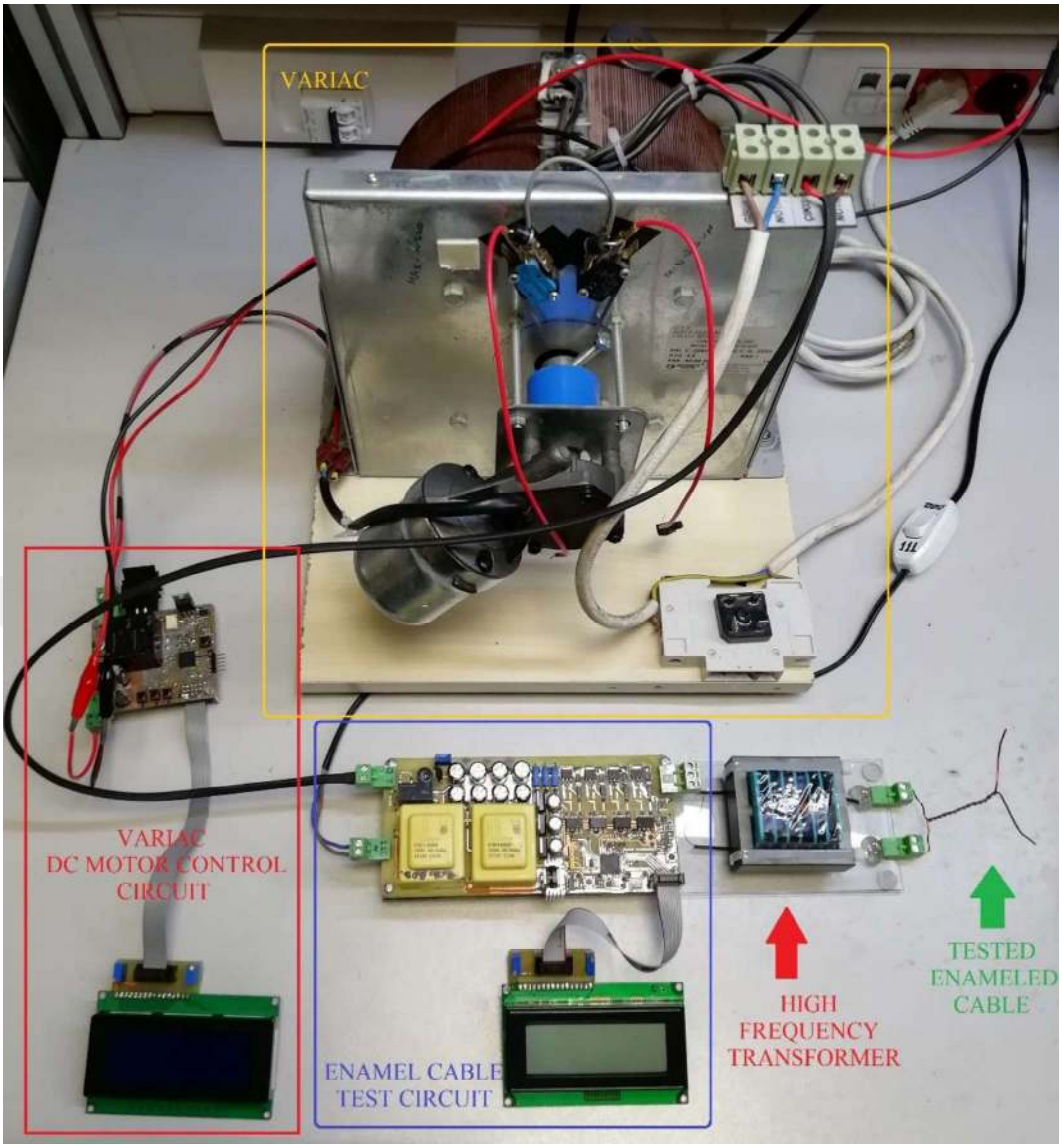

Figure 4.5 The experimental setup

4.3.1 Examination of Rectifying Voltage

It is very important for this system that the amount of oscillation of the rectified variac voltage that makes up the DC bus voltage of the H-Bridge switching circuit is low. Otherwise, a small amount of fluctuation in the primary voltage of the high frequency transformer (for example 3V) will cause a fluctuation of 60 V in the secondary voltage due to the high winding ratio of the transformer and therefore the error rate in our results will increase. Figure 4.6 shows the rectified variac voltage.

The oscilloscope output was taken when the variac voltage was at its peak and under 500 mA current. It is observed that there is some voltage drop due to variac.

Figure 4.6 Rectified variac voltage

4.3.2 Examination of MOSFET Signals

Under this heading, G-S and D-S voltages on power switches are examined. Since the four MOSFETs, drivers and driving resistors used on the H-Bridge are the same, only one switch is examined. . Figure 4.7 shows the G-S signal of the Q1 (H1) switch. The rise time (t_r) of the switch was measured approximately 120 ns. The Miller Effect caused by the C_{iss} and C_{rss} capacitors of MOSFET is clearly observed. Due to this effect, MOSFET's transmission time, that is turn-on time is approximately 60 ns.

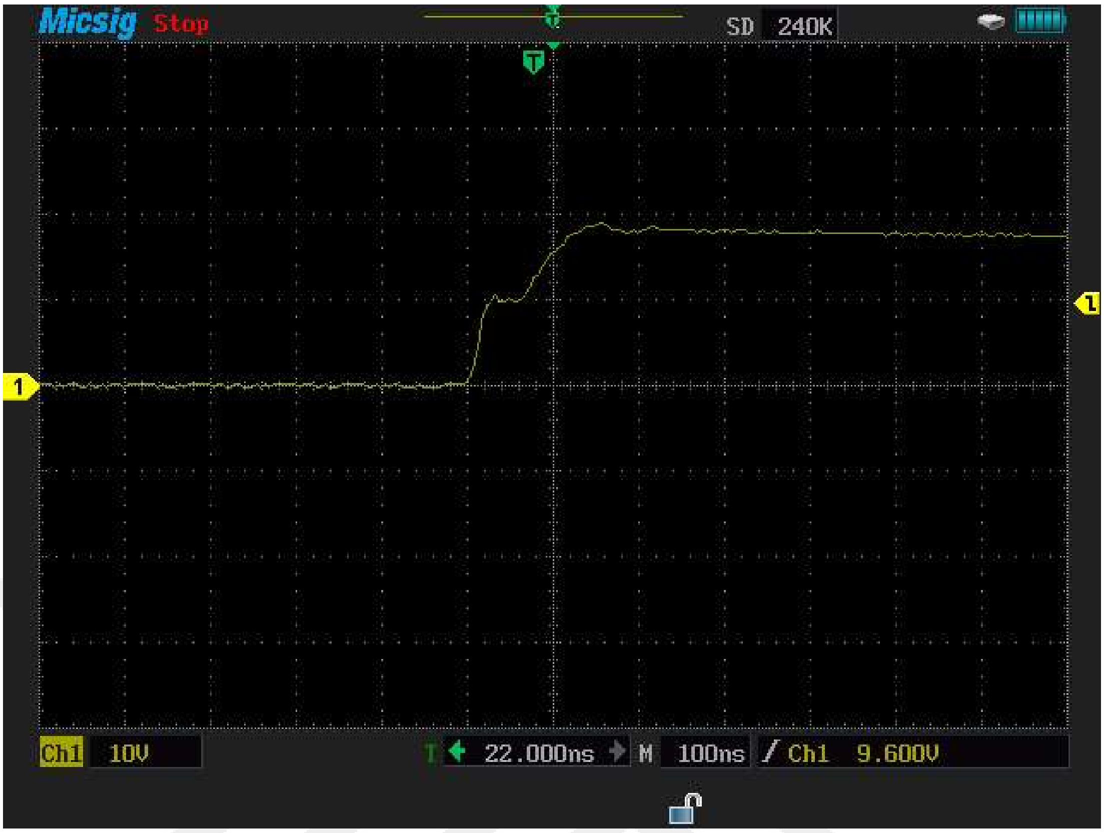

Figure 4.7 Q1 (H1) MOSFET G-S switching voltage

In Figure 4.8, G-S and D-S signals of the Q1 switch are seen together. The result obtained from this is that the snubber circuit performs its task quite well and MOSFET absorbs the high stresses that occur at the time of cutting. However, the capacitor of the snubber circuit is somewhat large. Therefore, MOSFET is slightly delayed and closes slowly. Snubber circuit capacitors can be reduced to eliminate this.

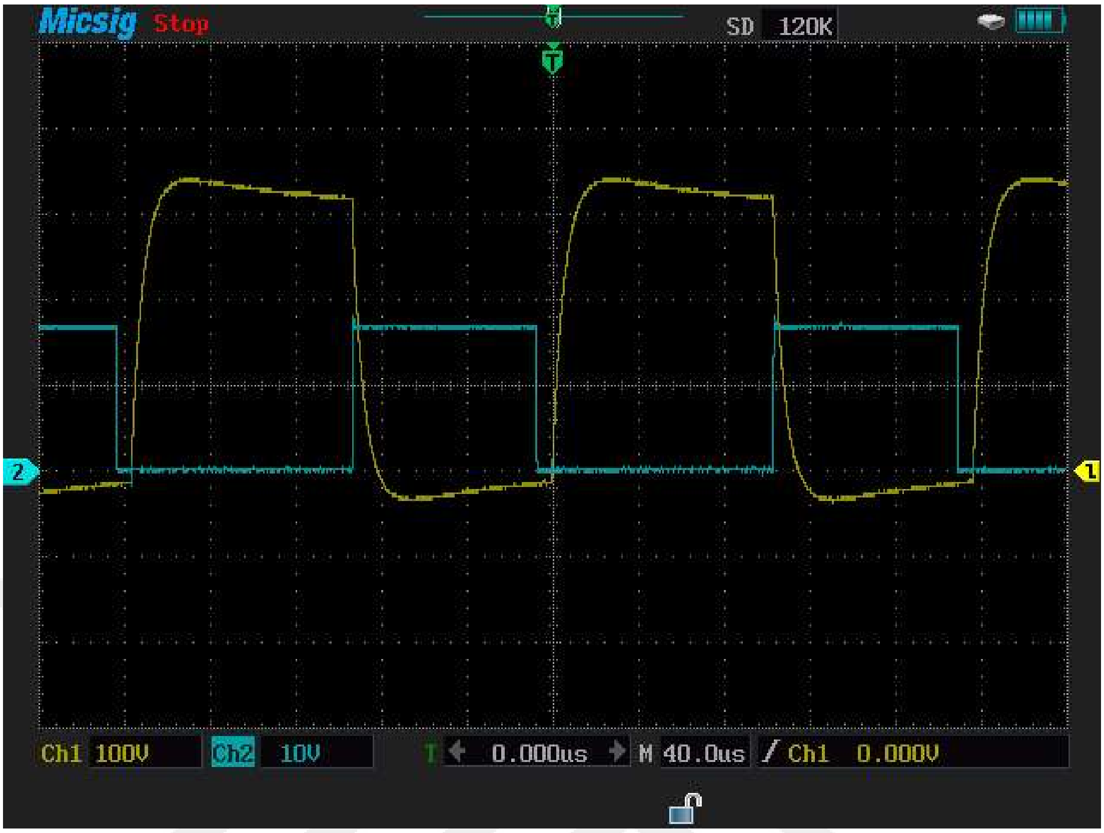

Figure 4.8 Comparison of G-S and D-S signals of Q1 MOSFET

4.3.3 Examination of Signs on High Frequency Transformer

Primary voltage of the high voltage transformer, which is one of the most important parts of the system, can be seen in Figure 4.9. It has been observed that the primary sign is also stress-free as a result of the switches being stress-free and smooth in the H-Bridge circuit.

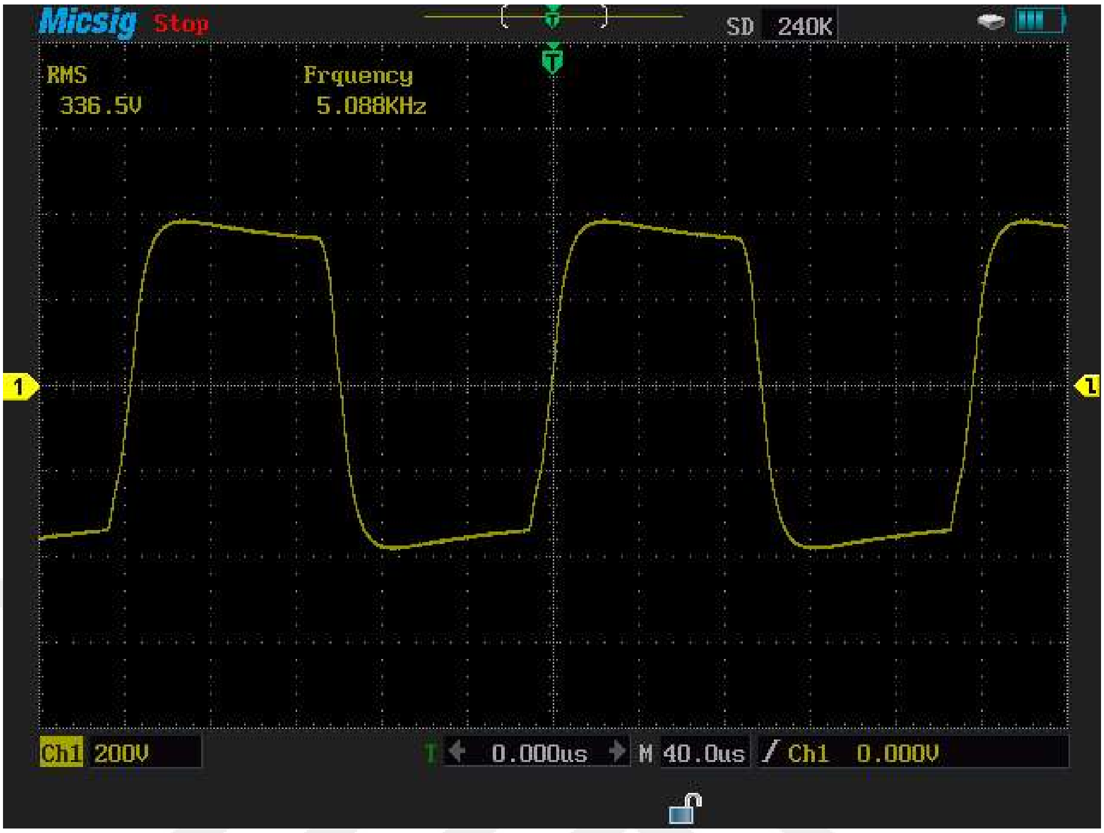

Figure 4.9 HVT primary winding voltage

Figure 4.10 shows the secondary voltage of the high voltage transformer. The secondary voltage seen here is the secondary voltage taken when the input voltage is 43 V. Due to the resonance of the stray capacitance and the stray inductance of the transformer, oscillations of about 80 V were observed at the peak and trough points. However, it has also been observed that these oscillations have no effect on the primary winding. Depending on the applied voltage, oscillations are negligible. In addition, in the first carcass study, it was observed that the secondary oscillations increased up to approximately 2000 V at the point where the DC bus voltage was 310 V. Again, in the first carcass study conducted in the same way, it was seen that there was approximately 40% oscillation when looking at the secondary voltage sign of the DC bus voltage at 43 V level.

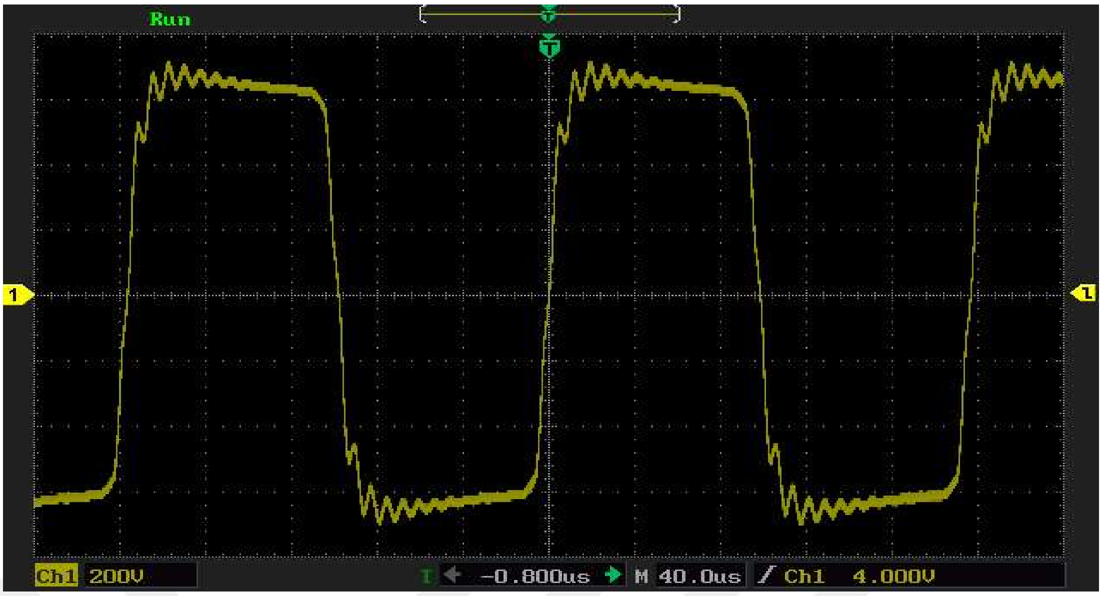

Figure 4.10 HVT secondary winding voltage

CHAPTER 5

CONCLUSION

As a result, 1 V - 5 kV / 1 Hz - 5 kHz AC square wave voltage obtained using H-Bridge switching circuit was applied to the enamel coated conductor and the puncture stress point of the coating was found. In this way, measurements can be taken at very high frequency values that cannot be obtained with the test devices already available in the market. In addition, the wires to be tested with this device have areas of use such as transformer windings exposed to high voltage. Thanks to the measurements taken with the device, it may be possible to say that much safer working conditions are provided in these areas.

During the tests, the voltage applied to the enamel coating was gradually increased with the condition of starting from the minimum point and the puncture voltage point of the coating was determined. The problems encountered during system design and experiment results and their solutions are listed below.

1. Since the number of windings in the secondary winding of the high frequency transformer connected to the H-Bridge switching circuit as a load is high, voltage jumps have occurred on the secondary winding as the voltage induced through the secondary winding is higher than the puncture voltage point of the enamel coating used in the transformer. Transformer carcass design has been changed to solve this problem. Primary and secondary windings are divided, and secondary windings are also divided into 5 separate compartments.
2. It has been observed that after the voltage applied to the tested conductor has reached a certain level (about 1000 V), the corona discharge begins to occur on the conductor. In addition, the enamel coating of the conductor under test has shortened the time the enamel will withstand partial discharge as the voltage / frequency value applied to the conductor increases.
3. While designing a high frequency transformer, firstly a method was tried in which the primary and secondary windings were wound separately and even

the secondary winding was divided into 5 sections within itself. The purpose of this design is to prevent voltage jumps between both the secondary windings and the primary and the secondary since high voltage is induced in the secondary winding. However, since this design increased the stray capacitance of the transformer, it caused oscillations of approximately 40% on the secondary voltage. For this reason, the classical transformer design has been reverted in which the primary winding is inside and the secondary winding is outside. However, voltage jumps have been observed in this design. This problem has been avoided by operating the high frequency transformer in the transformer oil.

REFERENCES

[1] Kaufholdg M., Borner G., Eberhardt M., Speck J., Failure Mechanism of the Interturn Insulation of Low Voltage Electric Machines Fed by Pulse Controlled Invertors. Conference on Electrical Insulation and Dielectric Phenomena, October 22-25, 1995.

[2] Yin W., Failure Mechanism of Winding Insulations in Inverter-Fed Motors, IEEE Electrical Insulation Magazine, 13(6), November-December, 1997.

[3] Fabiani D., Montanari G.C., Contin A., Aging Acceleration of Insulating Materials for Electrical Machine Windings Supplied by PWM in the Presence and in the Absence of Partial Discharges, IEEE 7th International Conference on Solid Dielectrics, June 25-29, 2001.

[4] Cavallini A., Conti M., Fabiani D, Montanari G.C., Evaluation of Corona-Resistant Magnet Wires Through Partial Discharge and Space Charge Measurements, Electrical Insulation Conference and Electrical Manufacturing and Coil Winding Conference, October 18, 2001.

[5] Fabiani. D., Relation between space charge accumulation and partial discharge activity in enameled wires under PWM-like voltage waveforms. IEEE Transactions on Dielectrics and Electrical Insulation, 11(3), 393-405, 2004.

[6] Ozaki T., Imai T., Sawa F., Shimizu T., Kanemitsu F., Partial Discharge Resistans Enameled Wire. Proceeding of 2005 International Symposium Electrical Insulation Materials, June 5-9, 2005.

[7] Haq S. U., Jayaram S. H., Cherney E. A., Evaluation of Medium Voltage Enameled Wire Exposed to Fast Repetitive Voltage Pulses. IEEE Transaction on Dielectrics and Electrical Insulation, 14(1) April, 2006.

[8] Cavallini A., Fabiani D., Montanari G.C., Tozzi M., The Influence of PWM Voltage Waveforms on Induction Motor Insulation Systems: Perspectives for the End User, 8th IEEE Symposium on Diagnostics for Electrical Machines, Power Electronics & Drives, September 5-8, 2011.

[9] Issı F., Topraklama Direncinin DsPıc Kullanılarak Sabit Tutulması Uygulaması. M. Sc. Thesis. Gazi University, 2013.

[10] Taylor D. J., Hızıroğlu H., Foss P.H., Breakdown and Partial Discharge Behavior of Enamel-Insulated Copper Conductors, IEEE International Conference on Solid Dielectrics, June, 2013.

[11] Wang P., The Influence of Repetitive Square Wave Voltage Parameters on Enameled Wire Endurance, IEEE Transaction on Dielectrics and Electrical Insulation, 21(3), June, 2014.

[12] Yıldız H. A., Güç Transformatörlerinde Kullanılan Katı ve Sıvı Yalıtım Malzemelerinin Özellikleri ve Alternatif Gerilimde Yalıtım Tasarımı. M. Sc. Thesis. Kocaeli University, 2014.

[13] Ota S., Yamauchi M., Mizoguchi A., Yoshida K, Tamura Y, Magnet Wire with Enhanced Tolerance for High Frequency Voltage, SEI Technical Review, 17(84), 97-101, 2017.

[14] Roger D., Ait-Amar S., Napieralska E., A method to reduce partial discharges in motor windings fed by PWM inverter, Open Physics, 1(16), 599-604, 2018.

[15] Ait-Amar S. Roger D. Mateo E. , An enameled wire with a semi-conductive layer: A Solution for a Better Distribution of the Voltage Stresses in Motor Windings, Open Physics, 1(17), 652-656, 2019.

[16] Borghei M., Ghassemi M, Partial Discharge Analysis under High-Frequency, Fast-Rise Square Wave Voltages in Silicone Gel: A Modeling Approach, Energies, 12(23), 4543-4556, 2019.

[17] Seri P., Giovanetti G., Zanotti L., Santoso H., Cavallini A., Mazzanti G., Partial Discharge Inception Voltage Characteristics at Low Frequencies: The Role of Electrostatic Charges, 2020 International Symposium on Electrical Insulating Materials (ISEIM), September 13-17,2020.

[18] Florkowski M., Influence of Insulating Material Properties on Partial Discharges at DC Voltage, Energies, 13(17), 4305-4323, 2020

[19] Pınarbaşı Aysun, Kablo Tanımı ve Yapısal Özellikleri 1. Bölüm, Kablosan Turkey, 2018: 112

[20] Aydın T., Bulanık Mantık Sınıflandırmadan Yararlanarak Kablo Malzemesi Seçimi, Thesis, İstanbul Technical University, May,2004.

[21] Horel C., Emaye Kaplı Tel Nedir? Nerelerde Kullanılır?, January 20, 2020, from https://malzemebilimi.net/emaye-kapli-tel-nedir-nerelerde-kullanilir.html

[22] Gülgör E., İzolasyon Cihazı Nedir? İzolasyon Test Cihazları, March 22, 2014, from https://www.elektrikport.com/teknik-kutuphane/izolasyon-direnci-nedir-izolasyon-test-cihazlari/11683#ad-image-0

[23] Department of Defence, USA, Method 301 DIELECTRIC WITHSTANDING VOLTAGE, MIL-STD-202G, 2002: 155-157

[24] Department of Defence, USA, Method 302 INSULATION RESISTANCE, MIL-STD-202G, (2002): 159-160

[25] Cirris Easy-Wire Ver: 8.6.0 Help Files

[26] Sedding H.G., Gupta B.K., McDermid W.M., Bromley J.C., Schwabe R., Levin D., Stein J. , High voltage DC ramp testing as a diagnostic of stator insulation condition, Conference Record of the 1988 IEEE International Symposium on DOI, October, 2004.

[27] Özçelik Ü. C., Battery Charge System with Full Bridge DC-DC Converter. M. SC. Thesis, Karabük University, July 2018.

[28] Kocaağa E., Desing and Implementation of 400 a Industrial Welding Machine. M. Sc. Thesis, Yıldırım Beyazıt University, March 2019.

[29] Erickson, R., &Maximovic, D. Fundamentals of Power Electronics (2nd ed.), Boston: Kluwer, 2004.

[30] Yang W., Wei X., Du Y., Hu L., Zhang L., Zhang O., Design of an Improved RCD Buffer Circuit for Full Bridge Circuit. AIP Conf. Proc. 1836, 020116. May, 2017.